Helsinki University of Technology Publications in Engineering Physics

Teknillisen korkeakoulun teknillisen fysiikan julkaisuja

Espoo 2004 TKK-F-A832

# OPTIMIZATION OF REFLECTOR AND TRANSDUCER PROPERTIES FOR SURFACE ACOUSTIC WAVE DEVICES ON 128° $LiNbO_3$

Saku Lehtonen

Dissertation for the degree of Doctor of Technology to be presented with due permission of the Department of Engineering Physics and Mathematics for public examination and debate in Auditorium F1 at Helsinki University of Technology (Espoo, Finland) on the 19th of November, 2004, at 12 o'clock noon.

Helsinki University of Technology
Department of Engineering Physics and Mathematics
Materials Physics Laboratory

Teknillinen korkeakoulu
Teknillisen fysiikan ja matematiikan osasto
Materiaalifysiikan laboratorio

Distribution:
Helsinki University of Technology
Materials Physics Laboratory
P.O. Box 2200
FIN-02015 HUT
Tel. +358-9-451-3163
Fax. +358-9-451-3164
E-mail: saku@focus.hut.fi


ISBN 951-22-7360-8 (printed)
ISBN 951-22-7361-6 (pdf)
ISSN 1456-3320

Otamedia Oy
Espoo 2004

HELSINKI UNIVERSITY OF TECHNOLOGY
P.O. BOX 1000, FIN-02015 HUT
http://www.hut.fi

ABSTRACT OF DOCTORAL DISSERTATION

Author Saku Petteri Lehtonen

Name of the dissertation

Optimization of reflector and transducer properties for surface acoustic wave devices on 128° LiNbO3

Date of manuscript 20.8.2004 | Date of the dissertation 19.11.2004

☐ Monograph ☑ Article dissertation (summary + original articles)

Department Engineering Physics and Mathematics
Laboratory Materials Physics Laboratory
Field of research Surface acoustic waves
Opponent(s) Dr. Clemens Ruppel
Supervisor Prof. Martti M. Salomaa
(Instructor) Docent Victor P. Plessky

Abstract

Aluminium grating structures used for reflecting surface acoustic waves (SAW) on 128° LiNbO3 are studied in this dissertation. The properties of gratings are obtained from simulated and measured frequency responses of tailored test structures. In the simulations, Green's functions are used to characterize the piezoelectric substrate, the finite element method (FEM) is applied for calculating the fields in the metallic electrodes, and the boundary element method (BEM) is employed at the interface. The majority of the simulated responses are obtained with a rigorous two-dimensional tool for finite structures.

The reflection and transmission coefficients of the grating are extracted applying time gating to the test structure responses. Both their amplitudes and phases are evaluated. The former is used for obtaining the reflectivity of the reflectors. Furthermore, energy comparisons serve to address the attenuation inside the gratings, and, for short reflectors, provide the means to estimate the performance of the gratings. A number of analysis methods are used for the extraction of parameters. The quantitative results, presented in the framework of the coupling-of-modes terminology, are given as a function of the electrode geometry.

The observed great difference in the reflectivity of narrow short-circuited electrodes and that of wide floating electrodes is exploited in novel unidirectional structures introduced. The great advantage of the unidirectional schemes proposed is the large critical dimension of the structures, allowing the use of standard optical lithography up to the frequencies 2.5-3 GHz. In particular, low-loss and wideband unidirectional transducers are demonstrated for 2.45 GHz.

Keywords SAW, grating, 128° LiNbO3, reflectivity, attenuation

UDC 534.87:537.228:621.396.2 | Number of pages 67

ISBN (printed) 951-22-7360-8 | ISBN (pdf) 951-22-7361-6

ISBN (others) | ISSN 1456-3320

Publisher Helsinki University of Technology / Materials Physics Laboratory

Print distribution

☑ The dissertation can be read at http://lib.hut.fi/Diss/

# Preface

This work was carried out in the Materials Physics Laboratory at Helsinki University of Technology in collaboration with Thales Microsonics SA (presently Temex Microsonics) SAW Design Bureau and GVR Trade SA, Neuchâtel, Switzerland, CMAP/ Ecole Polytechnique, Paris, France, and RF SAW, Inc, Richardson, TX, USA. In particular, I am indebted to Thales/Temex Microsonics (Sophia-Antipolis, France) for conferring TRANSD, the FEM/BEM-based simulation tool for the analysis of SAWs in finite electrode structures developed by Thales/Temex Microsonics SA in collaboration with CMAP/Ecole Polytechnique at the disposal of HUT for this research work.

During the years spent in the Materials Physics Laboratory, I have been privileged to work in an inspiring and dynamic environment with the atmosphere tuned by a wealth of spirited personalities.

In the SAW group of the laboratory, a number of characters deserve a recognition. Julius Koskela is acknowledged for his admirable literary taste and for paving the proper way for the rest of us towards the doctoral degree. Jouni Knuuttila and Tapani Makkonen are recognized as the two closest comrades-in-arms who have fought aside me the same windmills all the way. Jouni's crusade against the maladies of modern hierarchical society and the obstinate sardonic standpoint towards the outer world of Tapani have enriched countless moments of my life as a student in the Materials Physics Laboratory. Janne Salo is thanked for being, for me, an incarnation of a prosperous and ingenious scientist and a true European citizen, who full-heartedly enjoys his life irrespective of his whereabouts. Johanna Meltaus is thanked for her exemplary calm and for adding the feminine touch preventing the rest of us from turning into a horde of savages. Olli Holmgren is recognized for his impregnable devotion to physical excercises, which lead him to encourage all the laboratory crew to keep fit. Kimmo Kokkonen, a wizard with an amazing spectrum of insight into all possible experimental puzzles, is thanked for sharing his philosophical views and plenty of less organized ideas with our team. Pasi Tikka, is acknowledged for his capability to execute any plan faster than anybody else I ever met.

In addition to the SAW group, colleagues specializing in optics and theoretical materials physics have witnessed me struggle to find my way. Joyous moments were passed with my former roommate Sergei Popov, who taught me the poetry of Lermontov. I am grateful to Eero Noponen who repeatedly and calmly rescued me from data processing dead ends. Teemu Pohjola and Tero Heikkilä are recognized for sending off their families to provide premises for sauna evenings. Sami Virtanen is thanked for his altruism, which manifested in both his generous offers to assume the position of the driver in the sauna evenings and in his pursuance to instruct the next generation of research students. Tapio Simula, with his full-throated laughter, together with other young talents in the theory group, is definitely the person who has demonstrated to

me that research may be great fun.

I wish to collectively thank my former and present colleagues, including those already mentioned, for everyday dealings, the vivid lunch-time conversations in particular, which fairly seldom had anything to do with science.

I am also privileged for having had the opportunity to collaborate with Clinton Hartmann, an amazingly resourceful pioneer throughout his 35-year-long career in SAW business and one of today's most eminent figures in the field. I wish to acknowledge professor Ken-ya Hashimoto, who demonstrated his skills in cooking and his exceptional force of mind in early-morning lessons of SAW physics. Professor Ali-Reza Baghai-Wadji is the most hard-working person I have encountered so far, but as he is a man with genuine enthousiasm and genious towards mathematics, the work load appears not to be a great burden for him.

The conclusion of this work would not have been possible without generous support from two very important characters.

I am deeply grateful to my instructor Victor Plessky, who guided me through the research process. He is abundant in new ideas for research, he has the ability to convey the essential to the listener and, first of all, he was always there for my numerous questions and inquiries. Our discussions were never limited by the narrow bounds of science. In particular, I have learned to appreciate the earthly viewpoints, impinged with heartly sarcasm, arising from the legacy of the ideological education obligatory in another era. It has been a great privilege and joy to work together with Victor. I hope and trust that this Thesis is not the end of our collaboration.

As far as the practical issues of my Thesis work are concerned, I owe everything to my supervisor, Professor Martti Salomaa. During all these long years, he has had the resolution to encourage me to continue the work towards this goal. I dare say that, having a history of swaying determination, I would never have come this far without Professor Salomaa. I want to express my deep gratitude for his patience and his numerous efforts, including the necessary threatening and bribery, in favour of me and my work.

I would also take the opportunity to thank my family and Maija for supporting me in this endeavour without putting any pressure on me. I thank you for your belief in me, a belief I sometimes did not have myself. My Godfather, professor Pekka Hirvonen, who among other things represents my first model of a person with a doctoral degree, can take the credit for considering himself a source of an inspiration for me. And dear sister, I hope the best of luck for you in your efforts towards your PhD!

In this work, financial support was provided by the graduate school in Technical Physics (Academy of Finland), Helsinki University of Technology, the Nokia Foundation and the Foundation of Technology (Finland). I wish to thank all these quarters for contributions.

Espoo, 31 August 2004
Saku Lehtonen

# List of publications

This dissertation is a review of the author's work in the field of surface-acoustic wave technology. It consists of an overview and the following selection of publications in this field:

**I** S. Lehtonen, V. P. Plessky, J. Koskela, and M. M. Salomaa, "Second-harmonic reflectors on 128° $LiNbO_3$", *IEEE Transactions on Ultrasonics, Ferroelectrics, and Frequency Control* **50**, pp. 972–978 (2003).

**II** S. Lehtonen, V. P. Plessky, and M. M. Salomaa, "Short reflectors operating at the fundamental and second harmonics on 128° $LiNbO_3$", *IEEE Transactions on Ultrasonics, Ferroelectrics, and Frequency Control* **51**, pp. 343–351 (2004).

**III** S. Lehtonen, V. P. Plessky, N. Béreux, and M. M. Salomaa, "Minimum-loss short reflectors on 128° $LiNbO_3$", *IEEE Transactions on Ultrasonics, Ferroelectrics, and Frequency Control* **51**, pp. 1203–1205 (2004).

**IV** S. Lehtonen, V. P. Plessky, N. Béreux, and M. M. Salomaa, "Phases of the SAW reflection and transmission coefficients for short reflectors on 128° $LiNbO_3$", *IEEE Transactions on Ultrasonics, Ferroelectrics, and Frequency Control*, (accepted).

**V** S. Lehtonen, V. P. Plessky, C. S. Hartmann, and M. M. Salomaa, "Extraction of the SAW attenuation parameter in periodic reflecting gratings", *IEEE Transactions on Ultrasonics, Ferroelectrics, and Frequency Control*, (accepted).

**VI** S. Lehtonen, V. P. Plessky, C. S. Hartmann, and M. M. Salomaa, "Unidirectional SAW transducer for gigahertz frequencies", *IEEE Transactions on Ultrasonics, Ferroelectrics, and Frequency Control* **50**, pp. 1404–1406 (2003).

**VII** S. Lehtonen, V. P. Plessky, C. S. Hartmann, and M. M. Salomaa, "SPUDT filters for the 2.45 GHz ISM band", *IEEE Transactions on Ultrasonics, Ferroelectrics, and Frequency Control*, (accepted).

Throughout the overview, these publications are referred to by their Roman numerals.

# Author's contribution

The studies in this dissertion are a result of work carried out in the Materials Physics Laboratory at Helsinki University of Technology (HUT) during the years 2000–2004. All Papers were generated in collaboration with Victor P. Plessky (Papers I–II: Thales Microsonics, SAW Design Bureau, Neuchâtel, Switzerland; Papers III–VII: GVR Trade SA, Bevaix, Switzerland). In addition, Papers III–IV involve cooperation with Natacha Béreux of Ecole Polytechnique, Paris, France, and Papers V–VII are coauthored by Clinton S. Hartmann, RF SAW, Inc., Richardson, Texas, USA. William Steichen and Marc Solal of Temex Microsonics SA (formerly Thales), Sophia-Antipolis, France, are acknowledged for useful discussions and for conferring the FEM/BEM software at the disposal of HUT for the simulations carried out in this work.

The author has substantially contributed to the research in Papers I–VII. The author has carried out the simulations of finite structures in Papers I–II, while those in Papers III–IV and VI–VII were executed by the developers of the numerical tool employed. With the exception of the simulations for infinite periodic arrays in Paper I, the author has generated the test structure input data for the numerical simulations in the Papers and implemented the analysis methods of the measured and simulated responses used. He has also performed all programming related to the analysis and extracted all the results. All Papers were written by the author. The essential results of Papers I–IV and VI–VII have been presented in the annual IEEE Ultrasonics Symposia; those of Papers I–IV and VII by the author and those of Paper VI by V. P. Plessky.

# Contents

# 1 Introduction

Acoustic waves are displacement fields propagating in media. For human senses, a tangible manifestation of acoustic waves in a gas is the sound in air with the displacement component parallel to the propagation direction of the acoustic wave. In gases, the matter is randomly arranged, its density is low, and the particles are free to move in all directions. In the liquid state, the viscosity and high density of the matter constrain the possible trajectories of the particles. Waves on the surfaces of water systems, with the predominant component of the displacement perpendicular to the propagation direction along the surface, serve to illustrate the propagation of acoustic waves in liquids. In solids, the matter is arranged on the atomic level. If the energy of a wave propagating in a solid is not sufficient to violate the limits of elasticity, the wave does not give rise to permanent changes in the inner structure of the solid. The propagation of acoustic waves inside a volume of solid material is difficult to perceive. Thus, instead of directly observing bulk waves, surface phenomena are typically witnessed. The most prominent—and sometimes destructive—manifestations of acoustic waves in solids are earthquakes, originating from the movements of crustal plates due to tectonic forces. An acoustic wave whose energy is localized near the surface of a solid, such as the earthquake wave, is a *surface acoustic wave* (SAW).

## 1.1 Surface acoustic waves (SAWs)

Surface acoustic waves were discovered theoretically by Lord Rayleigh [1] in 1885. The wavelength of a surface acoustic wave on a crystalline substrate is typically of the order of $10^5$ less than that of electromagnetic waves at the same frequency. The contemporary discovery of piezoelectricity [2], even though the phenomenon remained a scientific curiosity until World War I, laid the foundation of crystal acoustics. In the first half of the $20^{\text{th}}$ century, the bulk acoustic wave (BAW) applications dominated. With the development of microwave technology, the exploitation of SAWs to accomplish microwave-circuit functions gained endorsement as an attractive possibility for miniaturization in circuit design. The major breakthrough was provided in 1965 by White and Voltmer who proposed an interdigital transducer (IDT) for direct generation and reception of SAWs on a piezoelectric substrate [3], offering the means for the utilization of SAWs in high-volume applications.

In addition to the Rayleigh wave, with the vibration confined to the plane defined by the surface normal and the propagation direction and with the amplitude of the vibration decaying into the bulk, other surface-bound wave modes are possible in anisotropic crystals. Experimental and numerical indications [4] suggested that in various crystal cuts, a predominantly shear-polarized wave having a component dissipating energy into the bulk may propagate. For many crystal orientations, it was found that such a leaky wave flows parallel to the surface and that the bulk compo-

nent is small enough such that the energy of the leaky wave is essentially concentrated within a few wavelengths of the surface [6, 7]. Leaky waves were identified by Engan *et al.* [5]. Later on, another leaky surface wave mode with the main vibration component along the propagation direction, a leaky longitudinal wave, was found [8] and characterized [9].

In piezoelectric materials, a mode may exist where the lattice vibration occurs in the surface plane, orthogonal to the propagation direction with the amplitude of the vibration decaying into the bulk. This shear-horizontal wave is often called the Bleustein-Gulyaev wave according to its two independent discoverers [10, 11].

All of these acoustic wave modes may exist in piezoelectric substrate materials but, for practical purposes, their coupling is large enough and their attenuation sufficiently small only for favourable materials properties occurring in particular crystal orientations. The most straightforward way for the excitation of SAWs is a metallic IDT, which is essentially an array of electrodes. For the characterization of devices utilizing SAWs, models describing the electromechanical coupling and the perturbations due to the electrodes are required. In the following, single-crystal substrate materials and models proposed for the SAW technology are briefly reviewed.

## 1.2 Substrate materials

Crystal acoustics focused in the early days on materials research. Crystalline quartz ($SiO_2$) was among the first piezoelectrics to be studied [2] and the first to be widely exploited. A wealth of knowledge of solids used in ultrasonics was accumulated in Europe, particularly in Switzerland and in Germany, summarized by Götz [12]. The early development of piezoelectricity and its applications [13] is reviewed in Ref. [14] and the properties of piezoelectric materials discovered in the beginning of the 40s are summarized in Ref. [15].

Even though $SiO_2$ is abundant in nature, there are only few regions from where quartz crystals of considerable size and perfection could be found. By World War II, the main supply was Brasil, and new production areas were not being found. The solution to this problem and the most significant development in the research of quartz after World War II was the introduction of an industrially viable process to generate synthetic quartz crystals. The work, building partly on the legacy of German wartime research efforts, was mainly carried out in the Brush Development Co. (USA), the Bell Telephone Laboratories (USA), and the General Electric Company Ltd. (Great Britain) [16–23]. Among other findings, the temperature-stable cuts discovered earlier [24] were verified [25] and crystal imperfections studied [26,27]. Since then, several research groups published studies of surface waves on quartz. For early work, see, *e. g.*, [28–33].

Quartz exhibits a low piezoelectric coupling which renders it suitable for applications requiring a narrow frequency bandwidth. Lithium niobate ($LiNbO_3$) and lithium tantalate ($LiTaO_3$) [34–36] are synthetic high-coupling materials widely used in current ultrasonics. The properties of $LiNbO_3$ are studied, *e. g.*, in Refs. [37–50], and

those of $LiTaO_3$ in Refs. [41,42,46,49–54]. In particular, the fundamental material constants for $LiNbO_3$ are given in [39,41,45–50] and those for $LiTaO_3$ in [41,46,49,50,53]. Using the material data, methods for finding new crystal cuts were proposed [4,6,7,55]. For $LiTaO_3$, the leaky-wave 36° Y-cut found by Nakamura *et al.* [56] was later replaced by the 42°-cut [57]. For $LiNbO_3$, the YZ Rayleigh-wave cut (Y-cut, Z-propagating) was accompanied by the 41° Y-cut [58] and 64° Y-cut [59] leaky-SAW orientations. In addition, a Rayleigh wave with a high coupling was predicted and observed to exist close to the 130° rotated Y-cut plane [59, 60]. Further investigations led to the discovery of the 128° Y-cut of $LiNbO_3$, where the coupling of the Rayleigh wave is strong and the level of spurious signals is suppressed [61].

Other piezoelectric materials have been proposed, such as the berlinite ($AlPO_4$) [62–70], gallium phosphate ($GaPO_4$) [70–74], bismuth germanium oxide ($Bi_{12}GeO_{20}$) [75], lithium tetraborate ($Li_2B_4O_7$) [76–78] and langasite ($La_3Ga_5SiO_{14}$) [79, 80]. Lithium tetraborate and langasite have piezoelectric couplings larger than that of quartz and lower than those of $LiNbO_3$ and $LiTaO_3$ [76, 81]. They have thus been proposed as substrates for intermediate-bandwidth applications. The use of $Li_2B_4O_7$ is extensively covered by patents and, therefore, langasite has attracted more attention recently. The fundamental constants for langasite have been published by several authors [79, 80, 82–93], and the data has been extensively used to investigate the properties of langasite for SAW applications [70, 88, 94–110]. Langanite ($La_3Ga_{5.5}Nb_{0.5}O_{14}$) [111–113] and langatate ($La_3Ga_{5.5}Ta_{0.5}O_{14}$) [114] are among the crystal compounds that belong to the same group. The properties of the former are reported in Refs. [70, 90–93, 103, 107, 113] and those of the latter in Refs. [90–93, 103, 107, 110, 115–120]. Recent discoveries include potassium niobate ($KNbO_3$), a piezoelectric material with crystal orientations exhibiting a very strong electromechanical coupling [121]. Research on $KNbO_3$ towards ultrasonic applications is still at an early stage [122–127].

## 1.3 Models for the characterization of SAWs and SAW devices

The analysis and design of SAW components is closely related to analyzing the propagation characteristics of a surface wave in a perturbed structure. Since the treatment of a problem of perturbations on a piezoelectric half-space is numerically intensive, the use of rigorous models in design has been limited until recently. In device design, the equivalent-circuit and transmission-line models used in the early characterization work [128–132] are to a large extent replaced by the phenomenological coupling-of-modes (COM) model [133], which was first proposed for SAWs by Koyamada and Yoshikawa [134], later independently applied by Chen and Haus [135], and generalized by Wright [136]. The advantages of the COM model include that the model produces feasible results, that only few parameters are needed to characterize SAWs in a periodic structure, and that the numerical operations are easy to implement and fast to execute. The shortcomings are that the COM model is inherently one-dimensional,

its accuracy depends on the accuracy of the input parameters, and that the model has a limited applicability to short structures where the end effects are prominent. The COM model was not anticipated to be usable for the characterization of leaky waves, but it has proven to produce remarkably good results. In this context, some improvements have been suggested to further enhance its accuracy [137].

Rigorous models, with a larger spectrum of physical phenomena related to the distribution of the SAW field in a grating incorporated and, consequently, with better accuracy, have been suggested. Their drawback is the considerably larger need for numerical processing time. Approaches for solving both the Green's function for a piezoelectric half-space and the effects of surface corrugation analytically [138, 139], and the numerical discretization of the problem of grating structures on a piezoelectric substrate [140, 141] have been addressed.

However, the majority of efforts has been focused on determining the parameters needed for the COM model from simulations of infinite periodic gratings. Experimental techniques are likely to yield most accurate results but the dependence of the relevant parameters on the electrode geometry and material properties renders the task laborious and expensive. In order to save resources, several numerical approaches have been implemented for the extraction of the COM parameters. A two-dimensional finite element method (FEM) has been used for characterizing one period of an infinite structure including both the metallic grating electrode and the piezoelectric substrate [142, 143], and a periodic Green's function analysis neglecting the mass loading of the electrodes has been proposed [144]. Accurate results have been obtained applying FEM to the electrode and characterizing the substrate with periodic or discrete Green's functions [145–147]. The boundary element method (BEM) may be used at the interface between the substrate and the electrodes.

The rapid increase in the capacity of computers has rendered more rigorous tools feasible. The current state of the art is two-dimensional FEM/BEM software for the characterization of finite structures, with arbitrary pattern along the length of the structure [148, 149], used for the characterization of device performance and for the extraction of COM parameters. The accuracy of this model is limited by the assumed infinite length of the electrodes and by the neglected transversal effects, such as diffraction and wave guiding. In some cases, the latter has been identified as the critical loss mechanism severely degrading device performance [150–152]. To include all acoustics in the models, FEM/BEM simulators using three-dimensional Green's functions are being developed.

## 1.4 Scope of the present work

In this Thesis, SAW structures on the 128° Y-rotated Rayleigh-wave cut of $LiNbO_3$ are investigated. 128° $LiNbO_3$ is standardly used in the SAW industry for TV filters due to its low level of spurious bulk wave responses, low attenuation, and high electroacoustical coupling. The same advantages also render 128° $LiNbO_3$ the preferred substrate for other solutions, *e. g.*, for SAW radio-frequency (RF) identification (ID).

In SAW ID tags, the interrogation signal is encoded by distrubuted partial reflections from a number of separate reflectors on the substrate surface.

RFID SAW tag systems are promising future applications for SAW technology. Contrary to the competing RFID solutions based on semiconductors, SAW tags are passive devices. No power source, such as a battery or a high-power carrier signal, is required for their operation. Thus, for SAW tags, a large reading distance and a miniature tag size are inherently available with low power levels. In modern SAW tag systems proposed, efficient SAW transduction and precise control of the amplitudes and phases of signals reflected from short reflectors are crucial.

Here, a rigorous 2D FEM/BEM tool [148,149] is used to characterize the operation of finite gratings and transducers on 128° $LiNbO_3$. Experimental measurements are carried out to verify the operation of tailored devices whose features build on the simulation results. Novel analysis methods are employed to extract numerical data on the structures studied.

In Papers I and II, the reflectivity and attenuation are considered in long and short reflectors, respectively. In Paper III, optimal geometries of short reflectors are proposed. Papers IV and V focus on the analysis of the amplitude reflection and transmission coefficients (R and T) of gratings. In Paper IV, the extraction of the phases of R and T for short gratings is discussed and, in Paper V, a direct method of determining the attenuation parameter from the ratio R/T is introduced. The quantitative results obtained for finite periodic gratings are presented in the framework of the COM model as a function of the electrode geometry. These findings are also utilized to realize novel approaches for functional SAW elements. Paper VI presents unidirectional transducer schemes feasible for mass production for high-frequency operation and Paper VII reports experimental results for filters utilizing the transducers introduced in Paper VI.

In the following, Chapter 2 concentrates on the realization and analysis of numerical experiments and measurements carried out to explore the properties of reflector gratings. Chapter 3 focuses on the methods of extraction of COM parameters, and Chapter 4 reviews the implementations of innovative directional devices, arising from the extracted properties of short structures. In Chapter 5, the results of this work and future prospects are discussed.

# 2 Analysis of reflector gratings

The analysis of the properties of interdigital transducers (IDTs) has attracted considerable attention ever since their discovery [3]. The first applications were delay lines consisting of two IDTs placed on the same acoustic track [153, 154]. In delay lines, the reflectivity of the IDTs gives rise to unwanted multiple-transit signals, out of which the triple-transit echo is the strongest and the most detrimental for the device performance. Within the IDTs, the constructive interference of waves reflected from the transducer electrodes result in significant reflections and nonzero scattering losses. In order to minimize the distortion imposed on the transducer response by these effects, a split-finger structure where the mechanical reflections are canceled was introduced [155].

In parallel, ways to exploit the distributed reflectivity of an IDT structure were investigated. A dispersive delay line consisting of two IDTs with a constant finger overlap, or aperture, and a changing periodicity along the length of the transducer was envisaged [156, 157]. The apodization technique, varying the electrode overlap along the length of an IDT, was introduced to SAW technology by Tancrell *et al.* [158, 159]. A long uniform IDT operating as a resonator was described theoretically and experimentally by Lakin *et al.* [160].

Although the IDTs could also be used for reflecting surface waves using an external tuning circuit [129,161], flexible realization of SAW devices called for rugged solutions for reflecting surface waves. A viable option was the metal strip grating introduced as a waveguiding structure by Sittig *et al.* [128] and first proposed to be used as a reflector and as a part of a SAW resonator by Ash [162]. Staples *et al.* [163] published the first theoretical and experimental results on SAW resonators using metal gratings on both sides of a short IDT to form a resonant acoustic cavity, followed by Joseph *et al.* [164]. Joseph and Lakin also proposed the two-port SAW resonator where, instead of one IDT, the acoustic cavity encompasses both an input and output IDT [165]. Dispersive reflection gratings with constant finger overlap and increasing periodicity were the functional part in reflective array compressors [166].

The properties of reflection gratings consisting either of metal strips or grooves were also studied. The transmission-line model proved convenient for the analysis of periodic arrays [128], and several methods to characterize the perturbation due to the grating were proposed [130–132, 167–173]. In addition, a technique based on applying the effective permittivity was presented for the analysis of infinite arrays [174]. Pioneering experimental work was performed by Szabo who studied the reflection and transmission properties of a short-circuited grating and evaluated the power losses [175]. Staples *et al.* proposed delay line test structures for studying the properties of a single grating or an acoustic cavity formed of two gratings and presented the frequency responses for the test structures [163]. Dunnrowicz *et al.* studied the reflection mechanisms of surface waves [176]. Experimental studies of the reflec-

tion and transmission properties of gratings on $LiNbO_3$ (the YZ and 128° cuts) and ST-quartz are reported, *e. g.*, in Refs. [131, 177–182]. Wright and Haus sought to fit an equivalent-circuit model to the experimental data [181, 183].

In this Thesis, the properties of gratings are studied via numerical experiments [148, 149] as a function of the electrode geometry. A weak propagation attenuation in the substrate, sufficient to account only for a fraction of the actual propagation loss, and the resistivity of the aluminium electrodes are included in the rigorous FEM/BEM simulations of long reflectors. For short reflectors, the intrinsic material losses are excluded from the Green's functions characterizing the substrate, and the resistivity is ignored. Paper I addresses the reflectivity and attenuation in long gratings, and Paper II those in short gratings. In Paper III, the optimum geometry for short gratings is discussed. Paper IV focuses on the phase changes attributed to the reflection from and transmission through short gratings.

## 2.1 Test structures

The test structures used for numerically investigating the properties of gratings are variants of that proposed by Wright [181]. The construct consists of a transmitting transducer connected to the electrical port 1, two receiving split-finger transducers (connected to the electrical ports 2 and 3), and a grating placed between the receiving transducers. The split-finger geometry in the receiving transducers is introduced to minimize the perturbation inflicted on the SAW [155] arising from the IDT at port 2. For long gratings, in order to distinguish the different time-domain signals registered at ports 2 and 3, gaps with different widths ($w_1$, $w_2$, $w_3$) between the elements of the test structure are used, see Fig. 2.1. For short gratings, to accurately compare the reflected and transmitted signals, the center-to-center distances between the elements in the test structure were chosen such that the partial signals reflected from and transmitted through the grating studied have identical propagation times, see Fig. 2.2.

The frequency bandwidth of an interdigital transducer, $\mathrm{BW_{IDT}}$, measured as the distance between the first zeros of the transfer function, can be estimated as

$$\mathrm{BW_{IDT}} = \frac{2}{N_{\text{finger pairs}}}. \tag{2.1}$$

Thus, choosing a small number of electrodes in the transmitting transducer (port 1) implies a wideband transducer response, and a large number of electrodes in the grating under investigation leads to a narrowband grating response. Consequently, for long reflectors, frequency-domain characteristics may be used to determine the reflector parameters. For an illustration of the response obtained for the test structure in Fig. 2.1 incorporating a long grating, see Fig. 3.1.

For a short grating, this approach is not feasible: the reflector properties are of wideband nature and the stopband is practically absent. Instead, one is obliged to estimate the reflectivity in the time domain. A relatively long input transducer and,

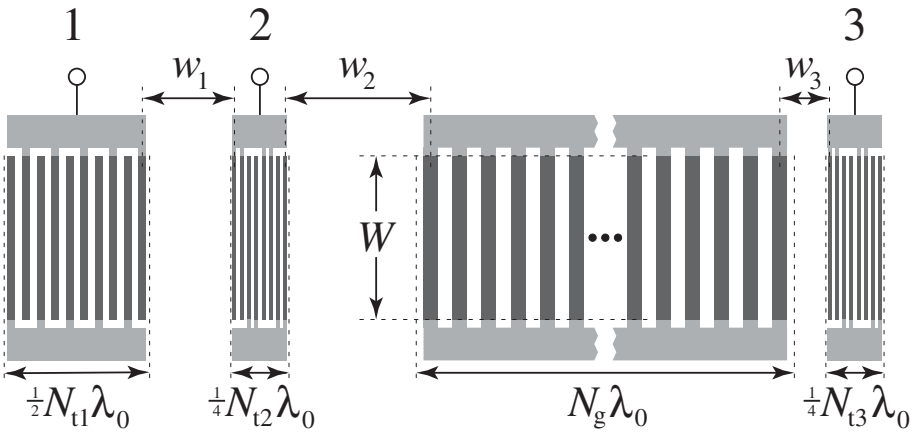


**Figure 2.1**: Test structure for numerical experiments of long gratings on 128° $LiNbO_3$. The values $N_{t1} = 10$, $N_{t2} = N_{t3} = 8$, $N_g = 80$, $\lambda_0 = 2$ $\mu$m, $W = 32$ $\mu$m, $w_1 = 100$ $\mu$m, $w_2 = 170$ $\mu$m, and $w_3 = 30$ $\mu$m are used. Here, gratings operating at the second harmonic frequency are illustrated ($p_{\text{grating}} = \lambda_0$). For the fundamental frequency, $p_{\text{grating}} = \lambda_0/2$ and $N_g = 160$.

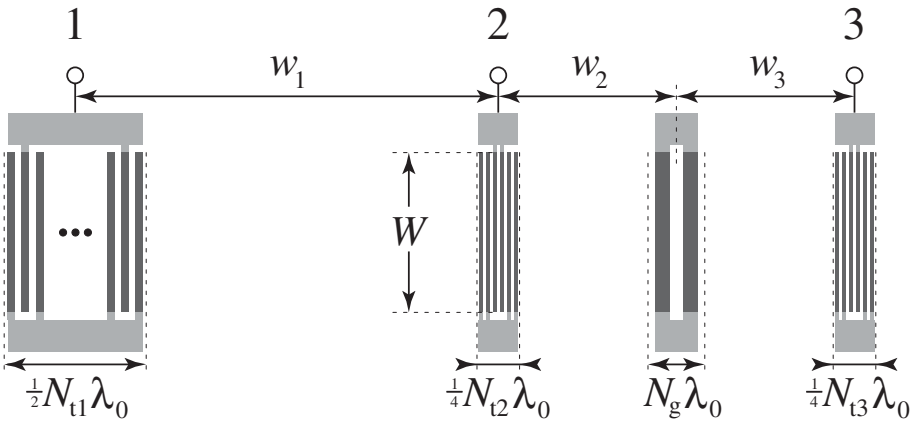


**Figure 2.2**: Test structures for numerical experiments of short gratings on 128° $LiNbO_3$. The values $N_{t1} = 21$, $N_{t2} = N_{t3} = 6$, $N_g = 1 \ldots 3$, $\lambda_0 = 1.6$ $\mu$m, $W = 200$ $\mu$m, $w_1 = 160$ $\mu$m, and $w_2 = w_3 = 64$ $\mu$m are used. Here, gratings operating at the second harmonic frequency are illustrated ($p_{\text{grating}} = \lambda_0$). For the fundamental frequency, $p_{\text{grating}} = \lambda_0/2$.

consequently, relatively long pulses with relatively narrow frequency bandwidths are used, and the amplitudes of the incident and reflected pulses are compared. According to Eq. (2.1), a long transducer produces a rather narrowband response. In the time domain, a reflected pulse is longer than the incident pulse due to the interaction with the reflector. If the reflector is short, the shape of the pulse is hardly changed: a short (wideband) reflector reflects nearly all the spectral components of a long (narrowband)

pulse. In such a case, the time-domain transition zones where the long incident pulse is entering and leaving the reflector are of minor importance in the reflection response. The shorter the reflector with respect to the transmitting transducer, the smaller the change in the shape of the pulse due to the reflection from the grating. In the case of a relatively long input transducer and a short reflector, the time-domain distortion is thus minimized.

## 2.2 Time gating

The FEM/BEM simulation tool used [148, 149] calculates the admittance matrix (Y parameters) of the specified electrode setup for a fixed frequency. To obtain a sampled frequency response, this procedure is repeated for N frequency points with constant spacing $\Delta$f. For the 3-port test structures used in the numerical experiments of this work (see Figs. 2.1–2.2), the outcome of the simulation is an N-element sequence of 3×3 admittance matrices, from which the interesting Y parameters, $Y_{21}(f)$ and $Y_{31}(f)$, may be selected.

The execution time of a simulation for a fixed frequency depends on the electrode setup. The desired simulation bandwidth B and frequency step $\Delta$f define the number of frequencies N analyzed by the simulation tool. The overall execution time equals N times the time needed to compute the characteristics of the structure at a single frequency point. The guidelines for selecting B, $\Delta$f, and the numbers of fingers in the different test structure elements are, on one hand, the aim to minimize the frequency and time dispersion caused by the grating to the incident signal and, on the other hand, a feasible simulation time.

The frequency-domain response obtained for the structure studied includes all the multiple reflections of the transmitted pulse. The 3rd and higher-order transit signals manifest themselves as ripples in the frequency stopband of the elements of the test structure. Here, time gating is employed to select the partial signals of interest from the simulated frequency responses. The discrete Fourier transform (DFT) is used for the time-domain analysis:

$$X(\omega_k) = \sum_{n=0}^{N-1} x(t_n) e^{-j\omega_k t_n}, \qquad k = 0, 1, \ldots, N-1, \tag{2.2}$$

where

$$\omega_k = \frac{2\pi k}{N\Delta t}, \tag{2.3}$$

$$t_n = n\,\Delta t. \tag{2.4}$$

Here, $x(t_n)$ is the discrete time series of input signal amplitudes at times $t = t_0, \ldots, t_{N-1}$; $\Delta t$ is the interval between subsequent time points; $X(\omega_k)$ is the complex-valued spectrum of the $x(t_n)$ at frequency $\omega_k$; and N is the number of both time and frequency

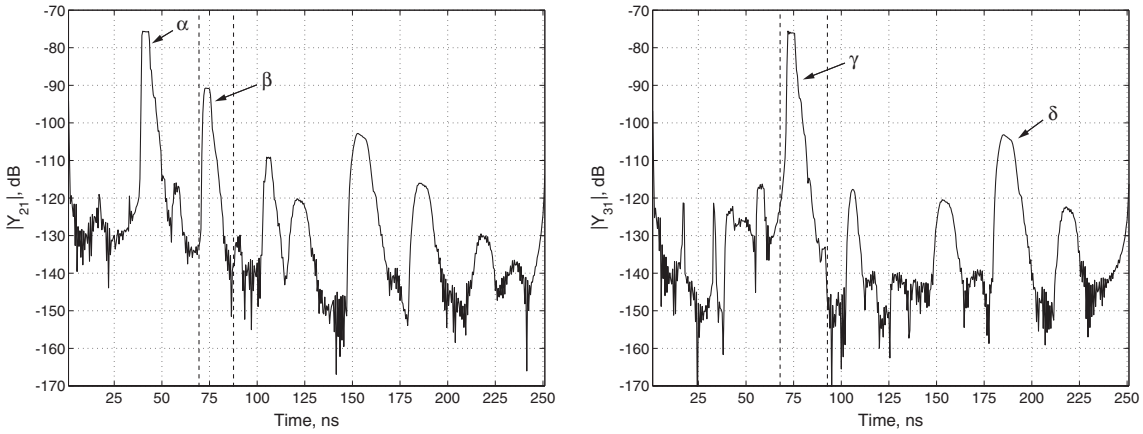


**Figure 2.3**: Magnitudes of the time-domain responses $|\mathrm{Y}_{21}|(\mathrm{t})$ and $|\mathrm{Y}_{31}|(\mathrm{t})$ for the test structure in Fig. 2.2. *Left*: Signal transmitted from port 1 and received at port 2. *Right*: Signal transmitted from port 1 and received at port 3. The vertical dashed lines confine the contributions of the direct signal (right) and the signal reflected once from the grating (left). The labels are explained in the text. Here, $a/p = 0.50$, $p = \lambda_0$, $h/\lambda_0 = 5\%$.

samples. The inverse DFT is given by

$$\mathrm{x}(\mathrm{t_n}) = \frac{1}{\mathrm{N}} \sum_{\mathrm{n}=0}^{\mathrm{N}-1} \mathrm{X}(\omega_\mathrm{k}) \mathrm{e}^{j\omega_\mathrm{k}\mathrm{t_n}}, \qquad \mathrm{n} = 0, 1, \ldots, \mathrm{N}-1. \tag{2.5}$$

From Eq. (2.3) one may relate the DFT frequency step $\Delta\mathrm{f}$ and the simulation bandwidth $\mathrm{B} = \mathrm{N}\Delta\mathrm{f}$ to the visible time scale $\mathrm{T} = \mathrm{N}\Delta\mathrm{t}$ and the time resolution $\Delta\mathrm{t}$:

$$\begin{aligned} \mathrm{T} &= \frac{1}{\Delta\mathrm{f}}, \\ \Delta\mathrm{t} &= \frac{1}{\mathrm{B}}. \end{aligned} \tag{2.6}$$

Here, the fast Fourier transform (FFT) [184], a method for efficiently computing the DFT, is used in the time-gating analysis. The inverse FFT is used to transform the Y parameter studied into the time domain. The temporal points corresponding to an identified pulse are maintained while the rest of the time response is set to a level close to zero. The FFT is then used to transform the truncated time-domain response back to the frequency domain. The time gating was first used for the analysis of SAW grating properties by Wright [181].

The direct and reflected signals are easily recognized in the time domain. Typical time-domain representations of the signals for the test structure in Fig. 2.2, observed at ports 2 and 3, are shown in Fig. 2.3. The left-hand-side plot of Fig. 2.3 displays the magnitude of the time-domain representation of $\mathrm{Y}_{21}$, *i.e.*, the signal transmitted by the input transducer at port 1 and received by the transducer at port 2. The labeled peaks indicate the partial signals corresponding to the direct SAW propagation from port 1 to port 2 (signal $\alpha$), and the propagation path to port 2 including a transmission through the receiving transducer at port 2 and a reflection from the reflector (signal

$\beta$). Similarily, the right-hand-side plot of Fig. 2.3 illustrates the magnitude of the time-domain representation of $Y_{31}$. The signal labeled $\gamma$ is the direct partial signal and the one labeled $\delta$ is the signal reflected once from the grating and once from the transmitting transducer. It is to be noted that due to the split-finger geometry of the receiving IDTs, the signals corresponding to reflections from ports 2 and 3 are strongly suppressed. In both figures, the vertical dashed lines indicate the truncation limits used in the time-gating procedure.

The source being in port 1, the admittances observed at ports 2 ($Y_{21}$) and 3 ($Y_{31}$) represent the electric currents at ports 2 and 3. Further, they are proportional to the corresponding acoustic-wave amplitudes. The time-gating procedure allows one to extract from $Y_{21}$ and $Y_{31}$ the contributions of the direct (incident) waves ($Y^{\mathrm{d}}_{21}$, $Y^{\mathrm{d}}_{31}$) and from $Y_{21}$ that of the wave reflected from the grating ($Y^{\mathrm{r}}_{21}$).

For short structures, the grating exhibits a small total reflectivity. Then the perturbation for waves passing through the split-finger IDT at port 2, even though minimized by the IDT geometry, may have a visible effect on the analysis results. Thus, the direct signal registered at port 3, obtained from a simulation of the operation of a test structure without the reflector, $Y^{\mathrm{d,\,ref}}_{31}$, is used as the reference signal. Contrary to choosing $Y^{\mathrm{d}}_{21}$ as a reference, the scattering from the receiving split-finger transducer at port 2 is then eliminated. Using the time-gated signal contributions, the frequency-dependent and complex-valued amplitude reflection and transmission coefficients of the grating are then

$$\mathrm{R(f)} = \frac{Y^{\mathrm{r}}_{21}(\mathrm{f})}{Y^{\mathrm{d,\,ref}}_{31}(\mathrm{f})}, \tag{2.7}$$

$$\mathrm{T(f)} = \frac{Y^{\mathrm{d}}_{31}(\mathrm{f})}{Y^{\mathrm{d,\,ref}}_{31}(\mathrm{f})}. \tag{2.8}$$

Here, the center of reflection is taken to be the center of the grating.

In order to obtain R and T, the frequency response of the device studied and that of the reference device are required. In simulations, this is only a matter of simulation time, but when experimental data is acquired, the possible inaccuracies in the two measurements degrade the results. However, the need of two separate measurements can be avoided by apprehending that the essential features of the reflection response are reproduced in the ratio of the reflection and transmission responses [185],

$$\frac{\mathrm{R(f)}}{\mathrm{T(f)}} = \frac{Y^{\mathrm{r}}_{21}(\mathrm{f})}{Y^{\mathrm{d}}_{31}(\mathrm{f})}. \tag{2.9}$$

For short reflectors imposing a limited distortion on the incident pulse, it is convenient to carry out the analysis of the phases of the signals in the time domain. Studying the phases of small signals in the time domain requires a high time resolution, which further necessitates a large frequency bandwidth. For example, the selection of a reasonable simulation bandwidth of 2 GHz with a 501-point grid ($\Delta f = 4$ MHz) results in the time resolution $\Delta t = 0.5$ ns, see Eq. (2.6). For aluminium electrodes on 128° $LiNbO_3$, the SAW velocity is close to 4000 m/s. The time resolution obtained

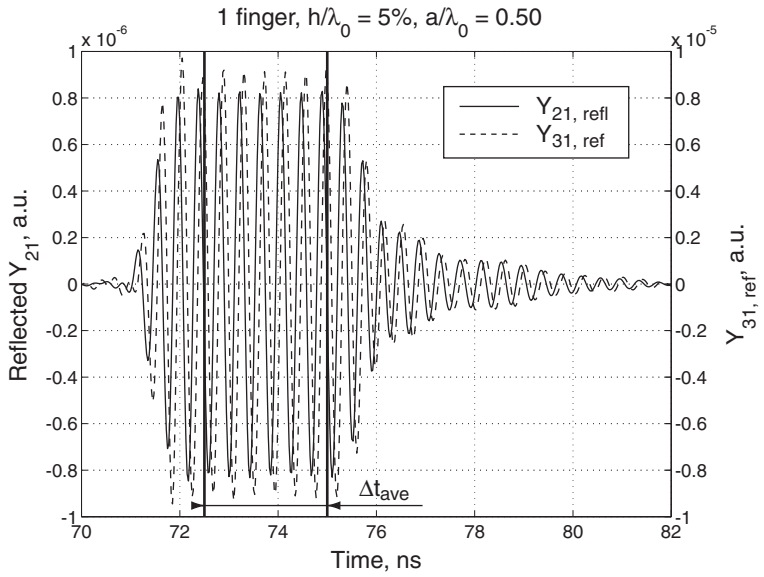


**Figure 2.4**: Reflected pulse ($\mathrm{Re}\{\mathrm{Y}_{21}^{\mathrm{r}}\}$) for a second-harmonic ($p/\lambda_0 = 1.0$) short-circuited electrode with $h/\lambda_0 = 5\%$ and $a/p = 0.50$. Note that the amplitude scales are different.

for the chosen frequency grid corresponds approximately to the SAW propagation distance of 4000 m/s $\cdot$ 0.5 ns = 2 $\mu$m, which is longer than the SAW wavelength at the center frequency ($\lambda_0 = 1.6$ $\mu$m). However, the phase changes attributed to the perturbation caused by the electrodes may be only a fraction of the full cycle. Thus, in order to extract reliable time-domain data on the phase of the waves reflected from and transmitted through the short grating, it is necessary to address the problematics of insufficient time resolution.

To render details of the time responses visible, the zero padding technique is used. Dummy points are continuously added to the simulated frequency response, maintaining the adopted frequency spacing $\Delta f = 4$ MHz. The time span T is not affected, see Eq. (2.6). The level of admittance of the dummy points is set close to zero in order not to distort the original response. By adding zeros to the frequency response in the regions where the signal is negligible, the simulated response remains physically intact, *i.e.*, no new information is added. In principle, such a wideband response could be calculated with the FEM/BEM software used [148, 149] but, knowing the signal to have a negligible amplitude in these frequency ranges, this procedure allows tremendous savings in the simulation time. Extending the bandwidth from 2 GHz to 40 GHz, the time resolution is enhanced to $\Delta t = 0.025$ ns (corresponding to the space resolution of 0.1 $\mu$m), which is sufficient for an approximate determination of the phases. An illustration of the time responses of the reflected and reference signals, with zero padding used, is shown in Fig. 2.4.

In the measurements, the typical output is S parameter data. For practical purposes, test structures consisting of two identical IDTs and a grating centered in the

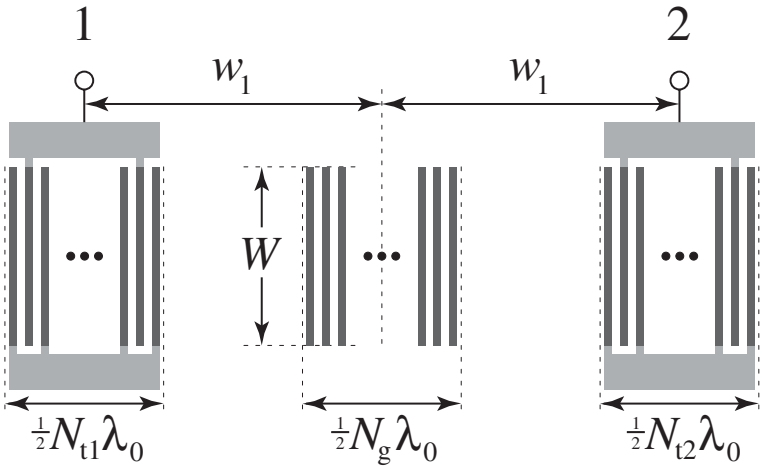


**Figure 2.5**: Schematic of the grating test structure used in the S parameter measurements. The distance between the centers of the transmitting and receiving IDTs ($N_{t1} = N_{t2} = 15$) is $2w_1 = 600$ $\mu$m and the aperture is $W = 100$ $\mu$m. Here, the grating has floating electrodes.

acoustic channel between them are convenient, see Fig. 2.5. One of the IDTs is then connected to the input and the other to the output, and two-port S parameter data is obtained. The time gating is needed to separate the signal contributions of interest. In the case of a grating with a large total reflectivity, however, the transmitted wave has a low amplitude and the truncation of the transmitted signal is not necessary. In such circumstances, the terms $Y_{21}^{r}$, $Y_{31}^{d}$, and $Y_{31}^{d,\,ref}$ in the above equations are to be replaced by $S_{11}^{r}$, $S_{21}$, and $S_{21}^{ref}$, respectively. Here, $Y_{21}^{d}$ does not have an S parameter counterpart.

## 2.3 Performance of a short grating

For short gratings, due to the test structure setup of Fig. 2.2, the propagation distances are equal for the partial signals corresponding to the reflection from ($Y_{21}^{r}$) and transmission through ($Y_{31}^{d}$) the grating. Furthermore, since the propagation attenuation of the SAW and the resistivity of the electrodes are excluded from the simulations, energy considerations of the two contributions ($Y_{21}^{r}$, $Y_{31}^{d}$) and the reference ($Y_{31}^{d,\,ref}$) then yield a means for the evaluation of the losses due to the scattering into the bulk [169]:

$$E_{sc}(f) = |Y_{31}^{d,\,ref}(f)|^2 - |Y_{31}^{d}(f)|^2 - |Y_{21}^{r}(f)|^2. \tag{2.10}$$

Low-loss structures may be found by comparing the scattering losses from Eq. (2.10) to the energy of the reference signal. This is not a sufficient criterion, though. Since the applicability of short gratings as reflecting elements is considered, one preferably needs to simultaneously attain a high or at least a moderate value for the reflectiv-

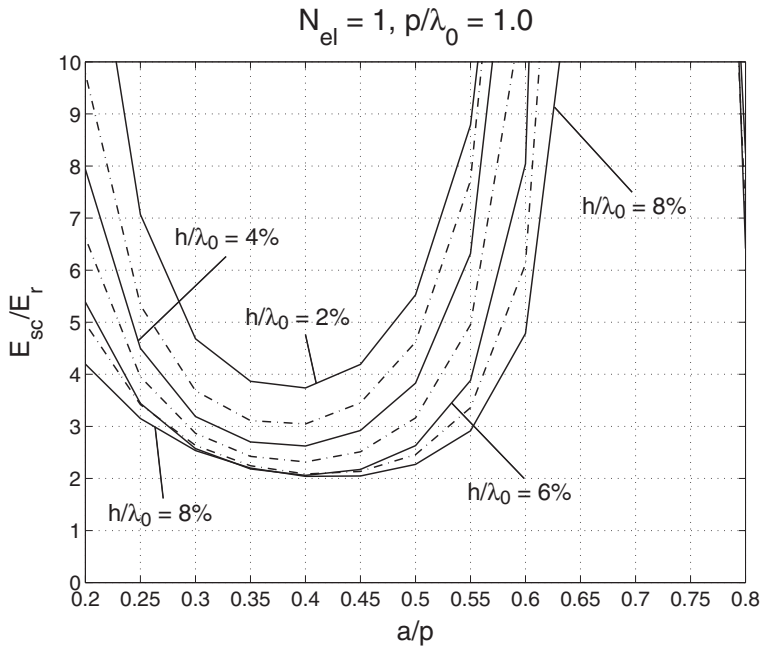


**Figure 2.6**: Ratio of the energy scattered into the bulk and the energy reflected for a single grounded electrode operating at the second harmonic frequency ($p = \lambda_0$) as a function of the aluminium thickness $h/\lambda_0$ and electrode width, expressed in terms of the metallisation ratio $a/p$.

ity and as small scattering losses as possible. These criteria can be addressed by considering the ratio of the scattered and reflected energies:

$$\frac{\mathrm{E_{sc}(f)}}{\mathrm{E_r(f)}} = \frac{|\mathrm{Y}_{31}^{\mathrm{d,\ ref}}(\mathrm{f})|^2 - |\mathrm{Y}_{31}^{\mathrm{d}}(\mathrm{f})|^2 - |\mathrm{Y}_{21}^{\mathrm{r}}(\mathrm{f})|^2}{|\mathrm{Y}_{21}^{\mathrm{r}}(\mathrm{f})|^2}. \tag{2.11}$$

The applicability range for short gratings on 128° $LiNbO_3$ is pronounced for the second-harmonic operation of grounded gratings. Figure 2.6 displaying the ratio of the scattered and reflected energies for a single grounded electrode as a function of the electrode thickness and width illustrates the optimum. Note that for a grounded single-electrode reflector, the energy scattered is more than twice the energy of the reflected wave. For a floating electrode, the ratio $\mathrm{E_{sc}/E_r}$ is slightly lower, and the situation improves significantly for 2- and 3-electrode open-circuited reflectors, see Paper III.

## 2.4 Phases of reflection and transmission coefficients

Phases of the reflection and transmission properties of gratings have not been reported widely in the literature. The early findings mainly concentrate on qualitative issues, such as the sign of the reflection coefficient. Cross found that for thin ($h/\lambda_0 \approx 0.2 \ldots 1.4\%$) aluminium electrodes on YZ-$LiNbO_3$, the electrical termination

condition affects the sign of the reflection coefficient [132]. Cambiaggio *et al.* studied the reflection and transmission coefficients of massless and perfectly conducting electrodes on YZ-$LiNbO_3$ and also deduced that the reflection phases differ for a single short-circuited and a floating strip [168]. Yamanouchi and Takeuchi proposed a novel reflector scheme employing interleaved gratings with positive and negative reflection characteristics [186, 187]. In particular, they predicted that for thin ($h/\lambda_0$ = 0 ... 2%) and narrow ($a/p$ = 0...0.5) aluminium electrodes on 128° $LiNbO_3$, the reflection contributions arising from the electrical and mechanical loading are in phase for a floating strip and out of phase for a short-circuited strip [187]. As a consequence, the total reflection coefficient for such a configuration features opposite signs for short-circuited and open-circuited conditions.

The reflection coefficient of a single electrode is often defined as $\mathrm{R} = -j\mathrm{R}_0$ [187]. For most materials, $\mathrm{R}_0$ is real and positive but, for the particular case of either open-circuited electrodes or shorted electrodes with a rather heavy mass loading on 128° $LiNbO_3$, $\mathrm{R}_0$ is negative and the phase of the reflection coefficient R is about +90° [187]. For clarity, the total reflection coefficient is referred to in this Thesis as $\mathrm{R} = |\mathrm{R}|e^{j\cdot\mathrm{Phase}}$.

In theoretical considerations of phases, the effect of finite losses is typically neglected. Conservation of energy implies that in a lossless case, the reflection and transmission coefficients are in phase quadrature ±90° [188]. The same result is obtained from the equivalent circuit model using the analysis of wave reflection from small impedance discontinuities [189]. However, when losses are included in the consideration, the phase difference between the reflection and transmission coefficients may differ from ±90°.

In this work, the phases of the reflected and transmitted signals are evaluated in both the frequency and time domains. In the former, the result is presented as a function of frequency in the vicinity of the center frequency (grating stopband),

$$\angle\left[\mathrm{R_f}\right] = \frac{360^\circ}{2\pi} \cdot \angle\left(\frac{\mathrm{Y}_{21}^{\mathrm{r}}(\mathrm{f})}{\mathrm{Y}_{31}^{\mathrm{d,\,ref}}(\mathrm{f})}\right), \tag{2.12}$$

$$\angle\left[\mathrm{T_f}\right] = \frac{360^\circ}{2\pi} \cdot \angle\left(\frac{\mathrm{Y}_{31}^{\mathrm{d}}(\mathrm{f})}{\mathrm{Y}_{31}^{\mathrm{d,\,ref}}(\mathrm{f})}\right). \tag{2.13}$$

In the time domain, the zero padding technique described in Sec. 2.2 is used, and values averaged over a time span corresponding to the interaction of the transmitted pulse with the receiving transducers (reflected pulse at port 2 and reference pulse at port 3) are given:

$$\angle\left[\mathrm{R_t}\right] = \frac{360^\circ}{2\pi} \cdot \mathrm{mean}\left\{\angle\left(\frac{\mathrm{Y}_{21}^{\mathrm{r}}(\mathrm{t})}{\mathrm{Y}_{31}^{\mathrm{d,\,ref}}(\mathrm{t})}\right)\right\}_{\Delta t_{\mathrm{ave}}}, \tag{2.14}$$

$$\angle\left[\mathrm{T_t}\right] = \frac{360^\circ}{2\pi} \cdot \mathrm{mean}\left\{\angle\left(\frac{\mathrm{Y}_{31}^{\mathrm{d}}(\mathrm{t})}{\mathrm{Y}_{31}^{\mathrm{d,\,ref}}(\mathrm{t})}\right)\right\}_{\Delta t_{\mathrm{ave}}}. \tag{2.15}$$

The averaging range is displayed in Fig. 2.4, where the phase difference between the incident and reflected pulses is illustrated.

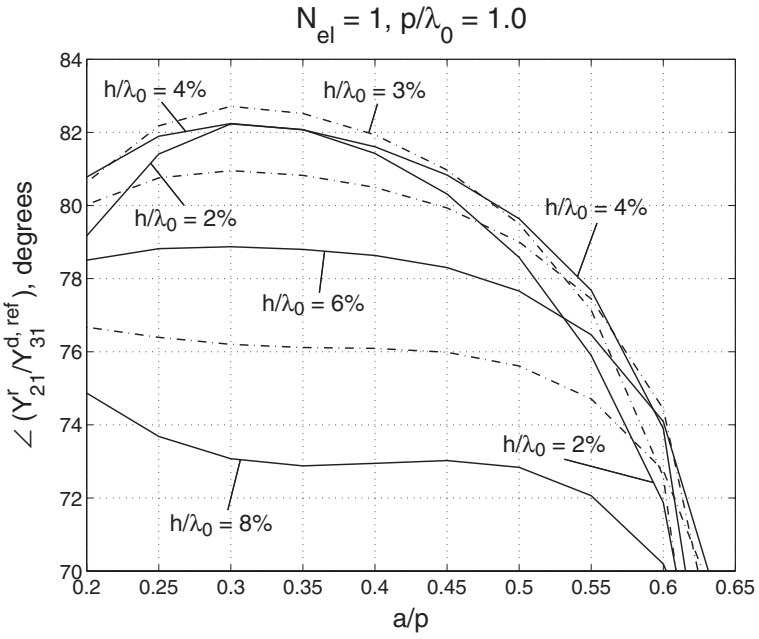


**Figure 2.7**: Phase of the reflection coefficient for a single grounded electrode evaluated in the time domain as a function of electrode width ($p = \lambda_0$).

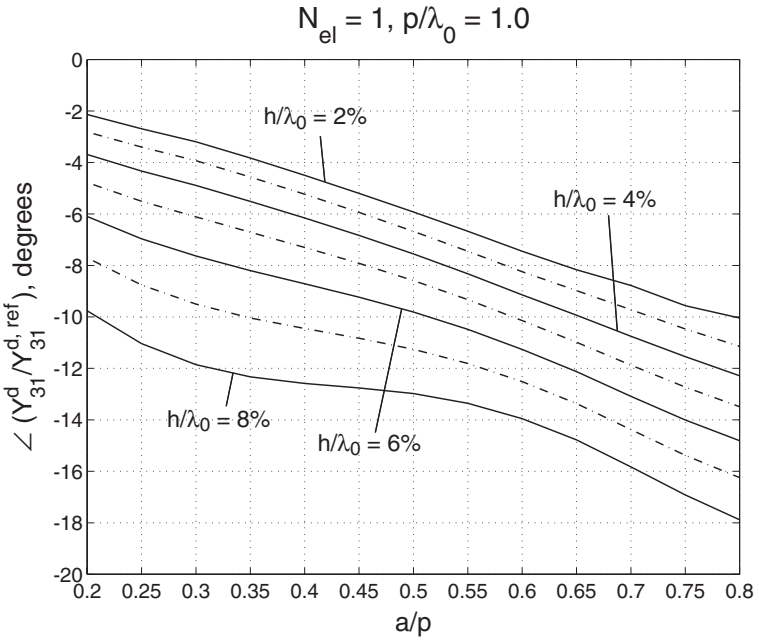


**Figure 2.8**: Phase change attributed to transmission through a single grounded electrode, evaluated in the time domain, as a function of the aluminium thickness $h/\lambda_0$ and electrode width ($p = \lambda_0$).

Examples of the extracted phases of the reflection and transmission coefficients for a single grounded electrode are plotted in Figs. 2.7 and 2.8. The dependence of the phases on the electrode geometry is demonstrated. Furthermore, comparing the plots, it is evident that the phase difference between the reflected and transmitted signals generally differs from $\pm 90^\circ$. This is attributed to the nonzero scattering losses evaluated from the simulated responses.

The phases of the reflection and transmission coefficients for various short gratings are discussed in Paper IV.

# 3 Extraction of the coupling-of-modes (COM) parameters

Despite the emergence of rigorous numerical simulators, the coupling-of-modes (COM) model [135,136] continues to be widely employed in SAW device design. It is a numerically fast method proven useful in the optimization of the geometry of SAW devices and, with current processing capacity of computers, it remains difficult to replace in the preliminary design stage. Moreover, with accurate input parameters, the COM model produces useful results. The materials-dependent COM parameters are the reflectivity $\kappa$, the electromechanical transduction $\alpha$, the velocity $v$, the attenuation $\gamma$, and the static capacitance $C$.

In this Thesis, the extraction of reflectivity and attenuation is considered. In Papers I and II, various methods for the extraction of reflectivity are implemented, and a technique based on energy comparisons is proposed for determining the attenuation. A large amount of data is presented as a function of the geometry of the grating electrodes. In Paper V, a method for the extraction of the COM attenuation parameter $\gamma\lambda_0$ from the characteristics of the grating response is introduced.

## 3.1 COM equations

According to the notation of Ref. [190], the COM reflection (R) and transmission (T) coefficients for a grating of length L are

$$\mathrm{R} = \frac{i\kappa^* \sin(\Delta \mathrm{L})}{\Delta \cos(\Delta \mathrm{L}) + i\delta \sin(\Delta \mathrm{L})}, \tag{3.1}$$

$$\mathrm{T} = \frac{\Delta}{\Delta \cos(\Delta \mathrm{L}) + i\delta \sin(\Delta \mathrm{L})}, \tag{3.2}$$

where

$$\delta = 2\pi \frac{\mathrm{f} - \mathrm{f_c}}{\mathrm{v}} - i\gamma = \delta_0 - i\gamma \tag{3.3}$$

is the frequency detuning with losses incorporated in $\gamma$, and

$$\Delta = \sqrt{\delta^2 - |\kappa|^2}. \tag{3.4}$$

Here, $\kappa$ is the reflectivity. The ratio of the reflection and transmission coefficients is obtained from Eqs. (3.1) and (3.2):

$$\frac{\mathrm{R}}{\mathrm{T}} = i\frac{\kappa^* \sin(\Delta \mathrm{L})}{\Delta}. \tag{3.5}$$

At the center frequency $\mathrm{f_c}$, the detuning $\delta_0$ in Eq. (3.3) equals zero. Estimates for the normalized reflectivity, $|\kappa\lambda_0|$, can be extracted from the center-frequency values

of the magnitudes of the reflection and transmission coefficients, or from the ratio |R/T|. For simple expressions, one may evaluate the lossless case ($\gamma = 0$ in Eq. (3.3)) from Eqs. (3.1), (3.2) and (3.5):

$$|\kappa\lambda_0|_{\mathrm{R}} = \frac{\lambda_0}{\mathrm{L}}\mathrm{atanh}(|\mathrm{R}(\mathrm{f_c})|), \tag{3.6}$$

$$|\kappa\lambda_0|_{\mathrm{T}} = \frac{\lambda_0}{\mathrm{L}}\mathrm{acosh}\left(\frac{1}{|\mathrm{T}(\mathrm{f_c})|}\right), \tag{3.7}$$

$$|\kappa\lambda_0|_{\mathrm{R/T}} = \frac{\lambda_0}{\mathrm{L}}\mathrm{asinh}\left(\left|\frac{\mathrm{R}(\mathrm{f_c})}{\mathrm{T}(\mathrm{f_c})}\right|\right). \tag{3.8}$$

However, nonzero attenuation affects the accuracy of the results. Inclusion of $\gamma$ in Eq. (3.3) leads to the expressions

$$\mathrm{R}(\mathrm{f_c}) = \frac{i\kappa^* \sinh(\Delta_\mathrm{c}\mathrm{L})}{\Delta_\mathrm{c}\cosh(\Delta_\mathrm{c}\mathrm{L}) + \gamma\sinh(\Delta_\mathrm{c}\mathrm{L})}, \tag{3.9}$$

$$\mathrm{T}(\mathrm{f_c}) = \frac{\Delta_\mathrm{c}}{\Delta_\mathrm{c}\cosh(\Delta_\mathrm{c}\mathrm{L}) + \gamma\sinh(\Delta_\mathrm{c}\mathrm{L})}, \tag{3.10}$$

$$\frac{\mathrm{R}(\mathrm{f_c})}{\mathrm{T}(\mathrm{f_c})} = \frac{i\kappa^* \sinh(\Delta_\mathrm{c}\mathrm{L})}{\Delta_\mathrm{c}}, \tag{3.11}$$

where

$$\Delta_\mathrm{c} = \sqrt{\gamma^2 + |\kappa|^2}. \tag{3.12}$$

In these formulae, the reflectivity $\kappa$ appears under the square root, together with the attenuation parameter $\gamma$. Solving Eqs. (3.9)–(3.11) requires the use of iterative methods.

## 3.2 Reflectivity

A number of methods may be applied to the extraction of reflectivity of gratings. The techniques differ for long and short reflectors.

The time-gated frequency response of the direct signal observed at port 3 ($|\mathrm{Y}^{\mathrm{d}}_{31}|$) for the long-grating test structure of Fig. 2.1 is depicted in Fig. 3.1. The most apparent difference with respect to the direct signal received at port 2 ($|\mathrm{Y}^{\mathrm{d}}_{21}|$, see Fig. 3.4) is the notch originating from the grating stopband. In addition, losses occurring at the transducers and along the propagation path between ports 2 and 3 lower the power level of the signal. The losses include the propagation attenuation both on the free surface and inside the grating, and the resistivity of the electrodes. Since the level of intrinsic material loss of the substrate, included in the simulation, is only a fraction of the actual experimental value, the free-surface propagation losses are negligible.

According to Eqs. (3.2) and (3.7), the reflectivity per wavelength $|\kappa\lambda_0|$ for a grating can be estimated from $\mathrm{Y}^{\mathrm{d}}_{31}$ (see Fig. 3.1) as

$$\mathrm{T} = \frac{1}{\cosh\left(|\kappa\lambda_0|\mathrm{L}(\lambda_0)\right)}, \tag{3.13}$$

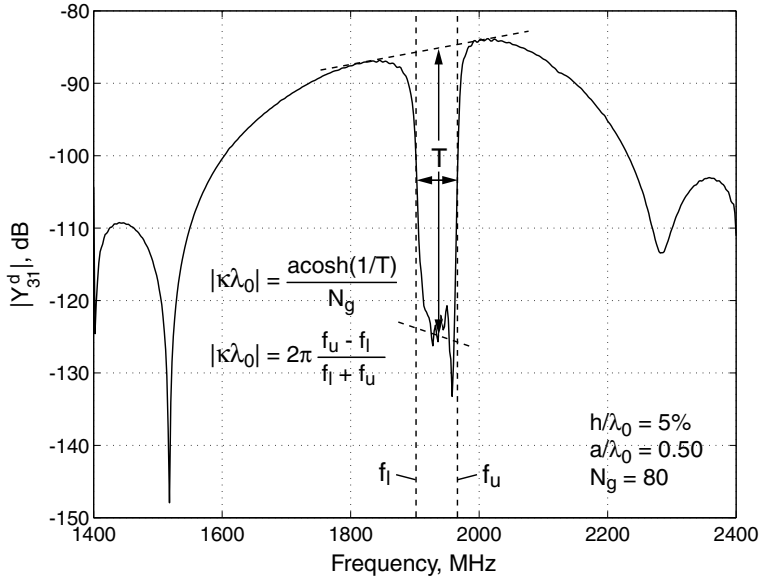


**Figure 3.1**: Direct signal contribution transmitted from port 1 and received at port 3 in the test structure of Fig. 2.1 in the frequency domain. The notch in the middle, a consequence of the grating stopband, is used to evaluate the reflectivity of the grating. Here, $a/p = 0.50$, $p = \lambda_0$ and $h/\lambda_0 = 5\%$.

where T is the amplitude transmission coefficient of the grating at the center of its stopband, and $\mathrm{L}(\lambda_0)$ is the length of the grating in units of $\lambda_0$. The grating is assumed to be long enough for the end effects to be negligible.

However, especially if the reflectivity is large, the depth of the notch in Fig. 3.1 is difficult to determine. This is due to the relatively low SAW amplitude, the stepsize of the frequency grid and the time-gating procedure. In order to obtain an improved approximation for $|\kappa\lambda_0|$, the width of the stopband is estimated from

$$\frac{|\kappa\lambda_0|}{\pi} = \frac{\mathrm{SBW}}{f_0} \Leftrightarrow |\kappa\lambda_0| = 2\pi\frac{f_\mathrm{u} - f_\mathrm{l}}{f_\mathrm{l} + f_\mathrm{u}}, \tag{3.14}$$

where $f_\mathrm{l}$ and $f_\mathrm{u}$ are the frequencies denoting the lower and upper edges of the stopband, respectively, and $\mathrm{SBW} = f_\mathrm{u} - f_\mathrm{l}$ stands for its width. Since the level at which the stopband is evaluated affects the result, an iteration procedure is employed where the expression for the above theoretical amplitude transmission coefficient is used to evaluate the actual minimum level at the notch and, further, the correct level for stopband width. For low total reflectivities, this method suffers from the large stepsize in the frequency grid, and Eq. (3.13) may be utilised as such, instead.

Another possibility is to investigate the notches of the reflection response, or those of the ratio R/T. As mentioned in the context of Eq. (2.9), the analysis of R/T necessitates a single two-port measurement and provides access to all essential grating features. In particular, the notches in |R/T| are found at the same frequencies as those of the reflection coefficient |R|. An example of the measured magnitude of the ratio

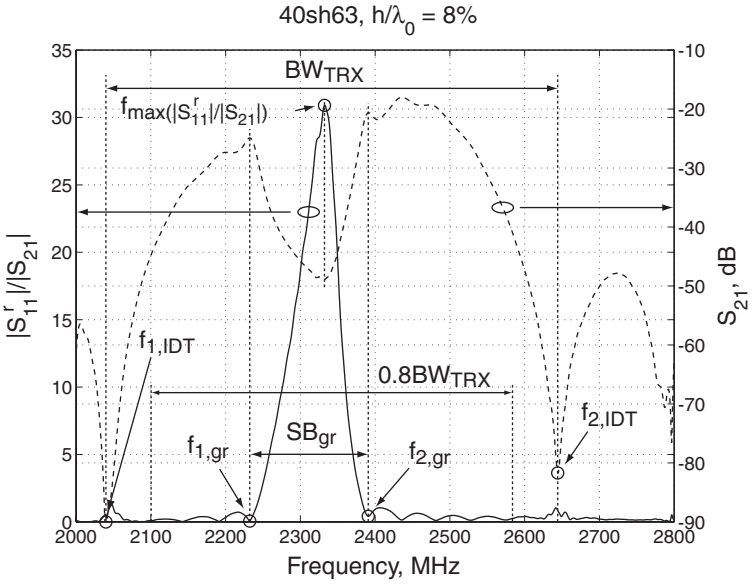


**Figure 3.2**: Response characteristics addressed when extracting the reflectivity of the grating. The solid curve is the ratio of the magnitudes of the reflection and transmission coefficients for a grating ($|\mathrm{R/T}| = |\mathrm{S}^{\mathrm{r}}_{11}|/|\mathrm{S}_{21}|$), where the first notches ($\mathrm{f}^{1}_{1,\mathrm{gr}}$ and $\mathrm{f}^{1}_{2,\mathrm{gr}}$) around the maximum ($\mathrm{f}_{\max(\mathrm{S}^{\mathrm{r}}_{11}|/|\mathrm{S}_{21}|)}$) define the grating stopband. The first notches of the transducer frequency response of the test structure (dashed curve, $\mathrm{f}_{1,\mathrm{IDT}}$ and $\mathrm{f}_{2,\mathrm{IDT}}$) indicate the range of feasibility. Here the grating within the test structure is short-circuited, and it has 40 electrodes with $a/p = 0.63$ ($p = \lambda_0/2$). The aluminium thickness $h/\lambda_0 = 8\%$.

of the reflection and transmission coefficients is shown in Fig. 3.2. The transmission response of the test structure of Fig. 2.5 illustrating the IDT characteristics (main lobe defined by the first notches $\mathrm{f}_{1,\mathrm{IDT}}$ and $\mathrm{f}_{2,\mathrm{IDT}}$) is also shown.

According to the lossless COM model, the notches in the magnitude of the reflection coefficient (and also those of $|\mathrm{R/T}|$) are found at

$$\frac{\Delta \mathrm{f}_n}{\mathrm{f_c}} = \sqrt{\left(\frac{|\kappa\lambda_0|}{2\pi}\right)^2 + \left(\frac{n\lambda_0}{2\mathrm{L}}\right)^2} = \sqrt{\left(\frac{|\kappa\lambda_0|}{2\pi}\right)^2 + \left(\frac{n}{\mathrm{N_{el}} - 1}\right)^2}, \tag{3.15}$$

where $|\Delta \mathrm{f}_n/\mathrm{f_c}|$ is the deviation of the $n^{\mathrm{th}}$ notch of $|\mathrm{R/T}|$ from the center frequency of the grating. Using the frequencies for the lower ($\mathrm{f}^{n}_{1,\mathrm{gr}}$) and upper ($\mathrm{f}^{n}_{2,\mathrm{gr}}$) notches, one may write

$$\frac{\Delta \mathrm{f}_n}{\mathrm{f_c}} = \frac{\mathrm{f}^{n}_{2,\mathrm{gr}} - \mathrm{f}^{n}_{1,\mathrm{gr}}}{\mathrm{f}^{n}_{1,\mathrm{gr}} + \mathrm{f}^{n}_{2,\mathrm{gr}}}. \tag{3.16}$$

The physical interpretation of Eq. (3.15) is that multiple reflections render the grating effectively shorter. For very long gratings, the waves do not penetrate up to the ends of the grating at the stopband frequencies. Then, the effect of the grating length is negligible. For short gratings, the term with $\mathrm{L}^2$ in the denominator

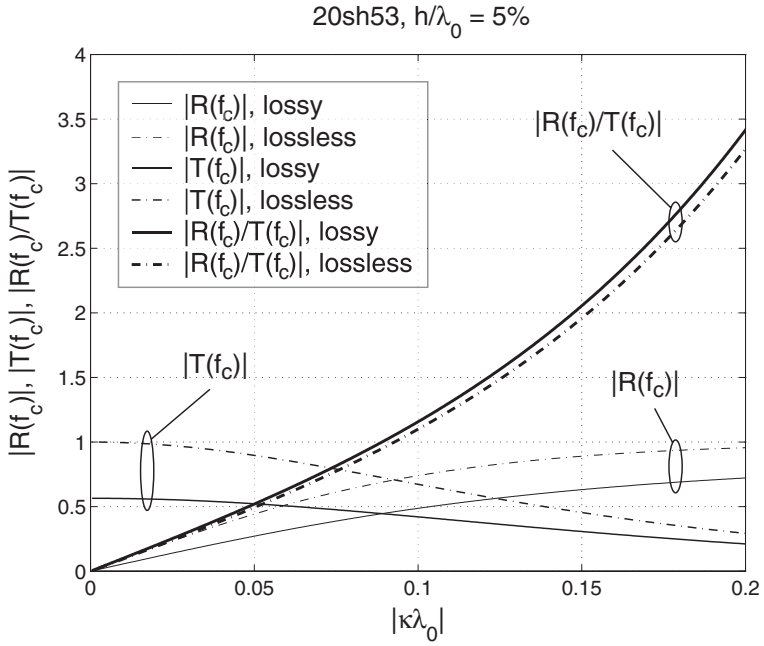


**Figure 3.3**: Dependences of $|R(f_c)|$, $|T(f_c)|$ and $|R(f_c)|/|T(f_c)|$ on $|\kappa\lambda_0|$ for the lossy and lossless cases.

dominates in Eq. (3.15). Extracting $|\kappa\lambda_0|$ from Eq. (3.15) implies the subtraction of two relatively large values to obtain a small value, which is disadvantageous for the accuracy. It is evident that Eq. (3.15) is accurate only if the term $(\lambda_0/2L)^2$ is small. Therefore, alternative methods are proposed for the extraction of the reflectivity of gratings to which Eq. (3.15) is not applicable.

In a case where the losses are chosen to be neglected, in addition to studying the amplitude transmission coefficient T of Eq. (3.13) or Eq. (3.7), the center-frequency values of the COM reflection coefficient in Eq. (3.6), or the property R/T, Eq. (3.8), may also be used for determining the reflectivity. Alternatively, the losses may be incorporated and one of Eqs. (3.9)–(3.11) used, but this leads to solving a transcendential equation numerically. The difficulty in the iterative procedure presented in Paper V is that the reflectivity and attenuation impose similar effects in the frequency response. If Eqs. (3.6)–(3.8) or (3.9)–(3.11) are used, comparison of the use of different identities in the extraction of reflectivity tends to favour the ratio R/T over the independent use of R or T. The difference between the lossless and lossy cases is evidently smallest for R/T as illustrated in Fig. 3.3.

The extraction of the reflectivity for short grating structures calls for an approach different from that applied to long reflectors. As opposed to a long reflector, the total reflectivity of a grating consisting of only a few electrodes is too low and of too wideband a character to produce a visible notch in the signal transmitted through the grating ($Y_{31}^{d}$). Instead, since the distortion originating from the interaction of the incident pulse with the short reflector is small, the reflectivity may be estimated in

the time domain.

A comparison of the levels of the reference signal ($|Y_{31}^{d,\,ref}(t)|$) and the signal reflected from the grating and registered at port 2 (reflected signal, $|Y_{21}^{r}(t)|$) in the time-domain representation of $Y_{21}$ provides an estimate for the reflectivity of short structures. Since the incident pulse has a definite duration due to the finite length of the transmitting transducer, see Fig. 2.3, the maximum values of the amplitudes of the direct and reflected signals are considered,

$$|\kappa\lambda_0| = \frac{1}{L_g(\lambda_0)} \frac{\max\{|Y_{21}^{r}(t)|\}}{\max\left\{|Y_{31}^{d,\,ref}(t)|\right\}}. \tag{3.17}$$

Here $L_g(\lambda_0)$ is the length of the grating in wavelengths. In the simulations of short reflectors, lossless Green's functions are used to characterize the substrate and the resistivity of the electrodes is excluded. The remaining loss mechanism is the scattering into the bulk inside the grating, which for short reflectors is predominantly an end effect.

## 3.3 Attenuation

The value of the COM attenuation parameter $\gamma$ is quite difficult to determine from the analysis of frequency responses. Within this Thesis, a method based on energy comparisons is proposed for the extraction of $\gamma$ due to the scattering. Another method is proposed for determining the COM attenuation parameter directly from the notches of the time-gated responses obtained from S parameter measurements of the test devices. The latter extraction procedure consists in studying the magnitude of the ratio of the COM reflection and transmission coefficients of the grating, R/T.

### 3.3.1 Energy comparisons

The attenuation due to scattering into the bulk may be evaluated from the scattering losses in Eq. (2.10). The amplitude attenuation value (in Nepers per wavelength) is then obtained through comparing the energy of the signal incident on the receiving transducer at port 2 of the test structure (Figs. 2.1–2.2) with the sum of energies of the contributions reflected from the grating (registered at port 2) and transmitted through the grating (registered at port 3). This comparison can be made at a single frequency point but a more reliable result is obtained by averaging over a frequency range $\Delta f$. For a long grating, the direct-signal reference at port 2 is $|Y_{21}^{d}|$ while for a short grating, $|Y_{31}^{d,\,ref}|$ is used, instead:

$$\gamma\lambda_0 = \frac{1}{2L_g(\lambda_0)} \cdot \text{mean}\left\{\ln\left(\frac{|Y_{31}^{d,\,ref}|^2}{|Y_{21}^{r}|^2 + |Y_{31}^{d}|^2}\right)\right\}_{\Delta f}. \tag{3.18}$$

Here, in order to define the COM attenuation coefficient per wavelength, $\gamma\lambda_0$, the losses are normalized to the length of the grating in $\lambda_0$, $L_g(\lambda_0)$.

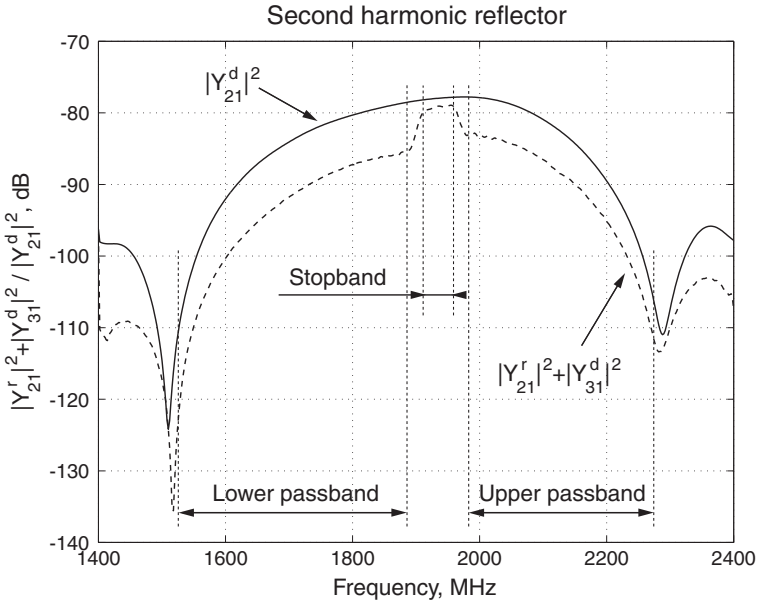


**Figure 3.4**: Energy balance for the structure shown in Fig. 2.1 with the reflector operating at the second harmonic frequency ($N_g = 80$, $p = \lambda_0$, $h/\lambda_0 = 5\%$, and $a/p = 0.5$). The dashed vertical lines indicate the grating stopband and the lower and upper passbands.

For a long grating, the total reflectivity may be strong. Especially, for the second-harmonic operation, the grating stopband clearly manifests itself in the energy balance picture Fig. 3.4. The attenuation values in the stopband and for the passbands, limited by the stopband edges and the zeros of the transmitted input signal, are evaluated separately, using different frequency intervals for the averaging. In the grating stopband, the wave does not penetrate through the whole length of the grating. Therefore, for the stopband frequencies — as opposed to the total grating length $\mathrm{L_g}(\lambda_0)$ — the losses are normalized to $|\kappa\lambda_0|^{-1}$, the effective penetration depth into the grating given by the COM model.

For short gratings, the total reflectivity is small with a wideband response but the averaging principle is similar. Since, due to the test structure geometry (see Fig. 2.2), the incident signal has narrowband character, we can estimate the scattering losses of our reflector only in a relatively narrow frequency band close to the center frequency of the input transducer, see Fig. 3.5. The averaging band $\Delta f$ is determined as the $-3$ dB bandwidth around the maximum of the reference $|\mathrm{Y}^{\mathrm{d,\,ref}}_{31}|$.

### 3.3.2 Ratio of the reflection and transmission responses

It is possible to deduce several properties of a grating by examining the behaviour of its frequency-dependent reflection coefficient, R. The values of the magnitude of R at the center frequency and at the minima are of particular interest. In a notch of the reflection response, the magnitude of the reflection coefficient attains a minimum,

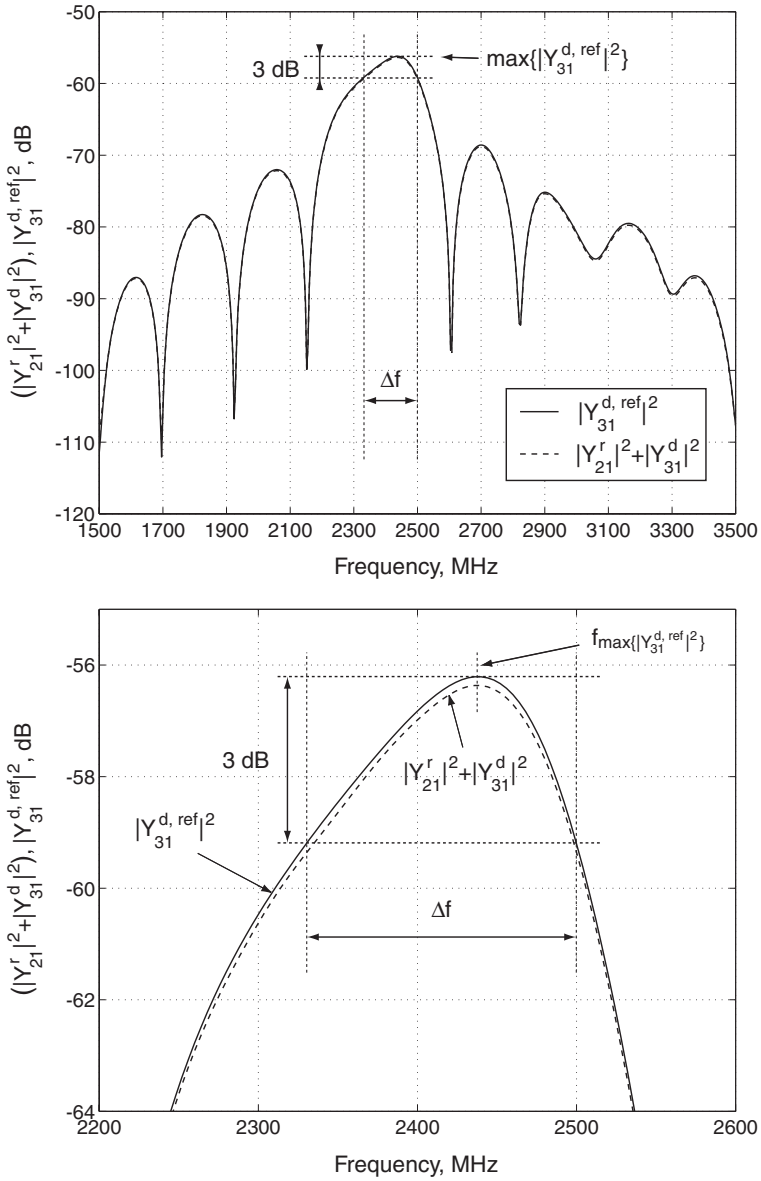


**Figure 3.5**: Energy balance for the structure shown in Fig. 2.2. *Above:* Total calculated response. *Below:* Detailed view. The dashed vertical lines indicate the averaging regime for the attenuation. Here, the reflector has 2 electrodes and second-harmonic geometry ($p = \lambda_0$). The aluminium thickness is $h/\lambda_0 = 5\%$ and the metallization ratio $a/p = 0.50$.

which requires that the vector sum of the contributions reflected from the grating electrodes is necessarily orthogonal with respect to the cumulative phase at the center frequency. A simplified illustration is the reflection from a one-dimensional array of perturbations, with multiple reflections and attenuation ignored. In a synchronous reflection, the partial reflected contributions $R_i$ add up in phase, see Fig. 3.6.

If the condition for the synchronous reflection is not met, there is a phase shift

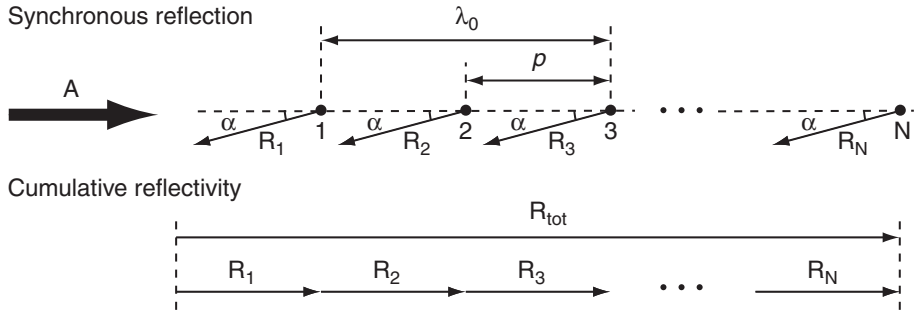


**Figure 3.6**: Schematic of the condition for synchronous reflection in the absence of multiple reflections. Here A is the amplitude of the incident signal and the partial reflected signals $\mathrm{R}_i$ of equal magnitude sum up in phase to yield the total reflected signal $\mathrm{R}_{\mathrm{tot}}$. The reference phase is $\alpha$.

between the subsequent partial contributions. Moreover, if attenuation is allowed, the amplitude of $\mathrm{R}_i$ decreases with increasing $i$. Then the cumulative vector diagram of Fig. 3.6 becomes curved with increasing curvature. Examples of cumulative reflectivities for a 40-element array are displayed for detunings close to the first and second notch of the reflection response in Fig. 3.7. The markers with black faces indicate the ends of the vector sums. In the absolute minima, the resultant sum vectors are orthogonal with respect to the incident signal.

As pointed out earlier, the essential characteristics of the reflection response are preserved when the ratio of the reflection and transmission coefficients is considered [185]. The advantages in studying R/T include that a single measurement is sufficient, Eq. (2.9), and that, in the COM framework, the phenomenological formulation is simple, compare Eqs. (3.1) and (3.5). In this Thesis, an analytic expression for the evaluation of the COM attenuation parameter $\gamma$ is derived [V].

On the assumption that the attenuation is not too strong ($\Delta^2|_{\mathrm{notch}} \gg \gamma^2$), $\Delta$ in Eq. (3.4) may be approximated at the $n^{\mathrm{th}}$ minimum of the reflection response as

$$\Delta_n \simeq \Delta_{0n} - i\frac{\delta_{0n}\gamma}{\Delta_{0n}}, \tag{3.19}$$

where

$$\begin{aligned} \delta_{0n} &= 2\pi\frac{\mathrm{f}_n - \mathrm{f}_{\mathrm{c}}}{\mathrm{v}}, \\ \Delta_{0n} &= \sqrt{\delta_{0n}^2 - |\kappa|^2} \simeq \pm\frac{n\pi}{\mathrm{L}} \\ \Rightarrow \delta_{0n} &\simeq \sqrt{|\kappa|^2 + \left(\frac{n\pi}{\mathrm{L}}\right)^2}. \end{aligned} \tag{3.20}$$

Substitution of Eq. (3.19) in Eq. (3.5) results in the expression

$$\left.\frac{\mathrm{R}}{\mathrm{T}}\right|_{\mathrm{notch}} \simeq i\frac{\kappa^*}{\Delta_{0n}}\sin\left(\Delta_{0n}\mathrm{L} - i\frac{\delta_{0n}\gamma\mathrm{L}}{\Delta_{0n}}\right), \tag{3.21}$$

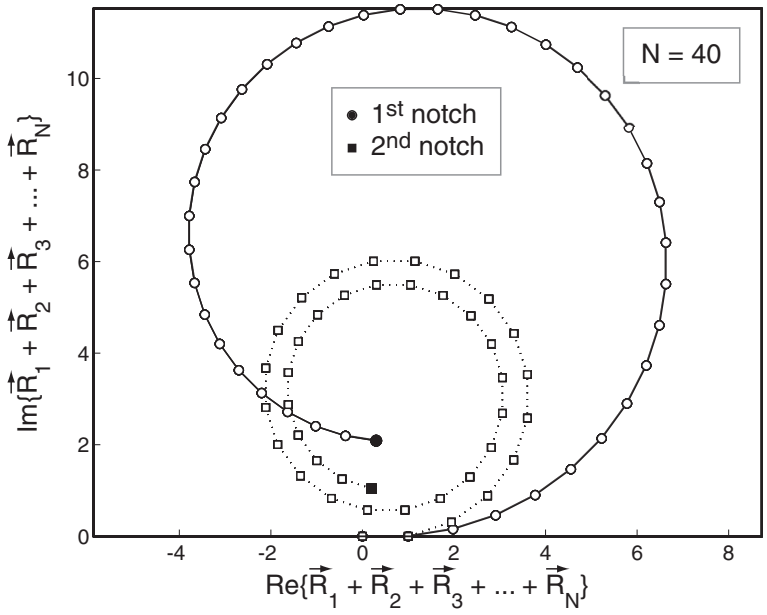


**Figure 3.7**: Schematic of the total reflection amplitude R in the vicinity of the first minima of the reflection response obtained as a vector sum for the asynchronous lossy condition. The circles (○) and squares (□) indicate the cumulative vector sum for detunings close to the first and second notches of the reflection response. Attempts to reduce R to the absolute minimum were not made.

which, assuming that the attenuation is not too strong, may be further reduced to the simple form

$$\left.\frac{\mathrm{R}}{\mathrm{T}}\right|_{\text{notch}} \simeq \pm\frac{\kappa^*\delta_{0n}\gamma\mathrm{L}^3}{n^2\pi^2}. \tag{3.22}$$

This expression indicates that the values of the magnitude of R/T at the notches are direct measures of the attenuation. Furthermore, it is interesting to observe that for low values of the reflectivity $\kappa$, $\delta_{0n}/n^2 \sim 1/n$, and the magnitude of R/T at the notches is inversely proportional to the notch order $n$. Moreover, for a real-valued reflectivity, the ratio R/T is purely imaginary for the center of the stopband while it is real at the minima, a property predicted by the simple model of an array of reflectors. Using Eq. (3.20) and denoting $\mathrm{f}_n - \mathrm{f}_\mathrm{c} = \Delta\mathrm{f}_n$, an expression is obtained where the reflectivity is normalized to the wavelength and the attenuation is associated with the grating length:

$$\left.\frac{\mathrm{R}}{\mathrm{T}}\right|_{\text{notch}} \simeq \pm\frac{2}{n^2\pi}\left(\frac{\Delta\mathrm{f}_n}{\mathrm{f}_\mathrm{c}}\right)\left(\frac{\mathrm{L}}{\lambda_0}\right)^2(\kappa^*\lambda_0)\,\gamma\mathrm{L}. \tag{3.23}$$

Here, Eq. (3.16) may be used for $|\Delta\mathrm{f}_n/\mathrm{f}_\mathrm{c}|$. For the fundamental mode of operation ($\lambda_0 = 2p$), the grating length is $\mathrm{L} = (\mathrm{N_{el}}-1)\lambda_0/2$. Then, Eq. (3.23) may be approximated

as

$$\left.\frac{\mathrm{R}}{\mathrm{T}}\right|_{\text{notch}}^{\text{fundamental}} \simeq \pm\frac{2}{n^2\pi}\left(\frac{\Delta \mathrm{f}_n}{\mathrm{f_c}}\right)\left(\frac{\mathrm{N_{el}}-1}{2}\right)^3 (\kappa^*\lambda_0)\,(\gamma\lambda_0), \tag{3.24}$$

and the attenuation normalized to the wavelength reads

$$\gamma\lambda_0 = \frac{4n^2\pi\left(\left|\frac{\mathrm{R}}{\mathrm{T}}\right|_{\text{notch}}^{\text{fundamental}}\right)}{\left|\frac{\Delta \mathrm{f}_n}{\mathrm{f_c}}\right|(\mathrm{N_{el}}-1)^3\,|\kappa\lambda_0|}. \tag{3.25}$$

It is interesting to note that a simple model for an asynchronous reflection in the array of reflectors of Fig. 3.6 yields an expression which closely resembles the result of Eq. (3.24) [V]. For a form independent of the normalized reflectivity, $|\kappa\lambda_0|$ may be inserted using Eq. (3.15). In the interest of accuracy, other methods for extracting the COM reflectivity are often preferable, see Sec. 3.2.

# 4 Novel unidirectional designs

The properties of short reflectors extracted within this Thesis [II] are employed to realize novel unidirectional devices for high-frequency operation [VI,VII]. The great advantage of the proposed structures over other schemes introduced is that they are feasible for standard optical lithography used in mass production. In the following, the background for unidirectional SAW device operation and the results obtained in this work are reviewed.

## 4.1 Unidirectional transducers

Interdigital transducers (IDTs) with uniform periodicity are bidirectional on the majority of substrates, *i.e.*, they radiate an equal amount of energy in both directions on the surface. For the commonly used substrates this implies that half of the energy input in a transducer is inherently lost. To overcome this shortcoming, unidirectional operation of an IDT was pursued. Engan proposed a structure composed of two identical IDTs separated by a distance $(n + \frac{1}{4})\lambda$ where $\lambda$ is the wavelength of the surface wave and $n$ is an integer [191]. The IDTs are then driven in phase quadrature such that the waves propagating in the forward direction add in phase while those propagating in the backward direction cancel. Collins *et al.* reported such a biphase transducer with a 6.5 dB insertion loss on YZ-$LiNbO_3$ [192]. The problem of this solution was the narrow bandwidth. Another approach used a meandering ground electrode between the fingers of an IDT, resulting in critical dimensions $\lambda/16$ wide and a rather high insertion loss [193]. The shortcoming of the three-phase unidirectional transducer with three electrode groups driven 120° out of phase, proposed by Hartmann *et al.* [194], was the need for multiple process steps in fabrication.

Other early design schemes suggested include the use of a multistrip coupler (MSC) [195], a coupling element for surface waves introduced by Marshall and Paige, which among other functions [196] was demonstrated to be suitable for achieving unidirectionality [197], and a hybrid-junction transducer consisting of two interleaved conventional IDTs [198]. The latter is essentially an extension of the three-phase unidirectional principle to four phases, involving the same complexity of fabrication. The MSC approach is not practical for substrates with low piezoelectric coupling, *e. g.*, quartz. Futhermore, its performance suffers from the parasitic losses in the MSC.

## 4.2 Single-phase unidirectional transducers (SPUDTs)

Single-phase unidirectional transducers (SPUDTs), first proposed by Hartmann *et al.* [199], were an important innovation. In SPUDTs, the internal reflections inside

the transducer are utilized to obtain a net unidirectional behaviour. In a unit cell of a periodic SPUDT structure, the centers of reflection are displaced by $\pm\lambda/8$ from the centers of transduction. A major advantage over multiphase schemes is the need for only one matching network. In the first configurations proposed [199], the directive operation was achieved using increased local reflectivity through additional mass-loading of alternate fingers in a split-finger structure. The selective increase of mass-loading necessitated an additional metallization step.

Another SPUDT approach builds on or is closely related to the idea envisaged by Hartmann *et al.* [199]. It uses a dielectric thin film to separate every second electrode of a split-finger IDT [200–202]. The directivity may be attributed to the variation in the electromechanical coupling along the structure due to the alternating separation of the electrode fingers from the piezoelectric substrate. For the different configurations reported, the performance remained poor compared to the response predicted.

Lewis [203] proposed a comb transducer structure encompassing a number of active IDTs connected to the same busbars and offset reflectors in the spaces between them. The evident advantage of this scheme is that only one processing step is required. Lewis reported a 2.7-dB insertion loss for a 100-MHz delay line filter consisting of two such comb transducers on the same acoustic track with their forward directions opposite to each other.

Wright discovered that in asymmetric piezoelectric orientations, the internal reflections inside an IDT shift the centers of reflection and transduction from their implicitly assumed positions [204]. Therefore, for carefully chosen crystal orientations, the requirement that the separation between the transduction and reflection centers be $\lambda/8$ can be met for a symmetric IDT structure. Such unidirectionality, originating from the asymmetry of the piezoelectric crystal, is referred to as natural unidirectionality. Correspondingly, the symmetric transducers exploiting this property are referred to as NSPUDTs. The disadvantage of the NSPUDT orientations is that in order to achieve a reverse directionality on the same crystal cut, the metallization has to be changed.

The need to enhance the control of the internal reflections inside a transducer incited the development of the distributed acoustic reflection transducer (DART) [205]. In the DART unit cell, a gap between two fingers with the same polarity in a split-finger scheme is partly metallized, the variation being in the direction of the fingers. Thus the mechanical reflectivity of the electrodes and the electrical regeneration effect may be treated separately. An extension of the DART structure is the electrode-width-controlled (EWC) SPUDT where the distributed reflectivity inside a unit cell is controlled by varying the widths of the electrodes [206, 207]. More complex single-level unidirectional unit cell configurations comprising, in addition to the transducer fingers, floating and short-circuited metal strips were also proposed [201, 208–211] but the insertion losses of the prototype devices were unacceptably high. A thorough theoretical analysis of the basic structure [208] was presented in Ref. [212].

A further advance in the SPUDT design was the introduction of the resonant

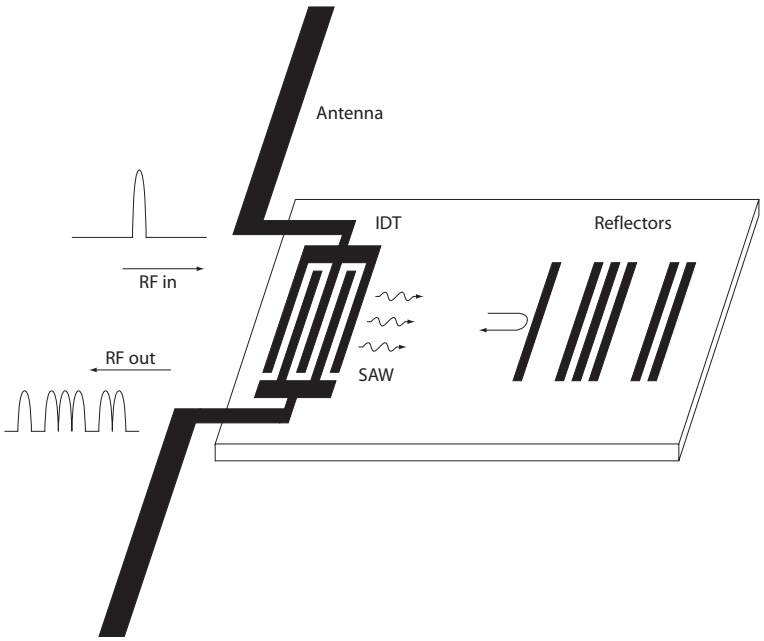


**Figure 4.1**: Schematic of a SAW ID tag; adapted from Ref. [215].

SPUDT (RSPUDT) [213]. In the resonant SPUDT structure, local resonant cavities are implemented inside the transducer while the overall unidirectionality is maintained.

SPUDTs are widely used in delay lines where slanted geometries are often implemented to achieve wideband operation. Another feasible application is wireless interrogation, where SPUDTs are envisaged as transducers in SAW identification (ID) tags [214, 215]. Radio-frequency (RF) ID tags are challenging the bar codes since they need no optical path, they work in a dirty environment and, first of all, they are insensitive to the orientation and enable a large reading distance. SAW tags, in contrary to approaches based on semiconductors, are passive devices, which need no battery or other source of power. In a SAW tag, the input signal is received by an antenna, converted into an acoustic wave and launched by a transducer, encoded by SAW reflections, and reconverted into an electric signal by a transducer and retransmitted by an antenna. The typical solution uses a single acoustic channel with the antenna and transducer used for both receiving and transmitting the radio signal, see Fig. 4.1. Other solutions using several channels have been proposed, see, *e. g.*, Ref. [216]. As reflectors, split-finger transducers [215] or various gratings [216] may be used.

## 4.3 SPUDT configuration for the gigahertz regime

The main disadvantage in the majority of the single-level SPUDT designs is that they use $\lambda/8$-wide or narrower electrodes or gaps. In the gigahertz range, the critical

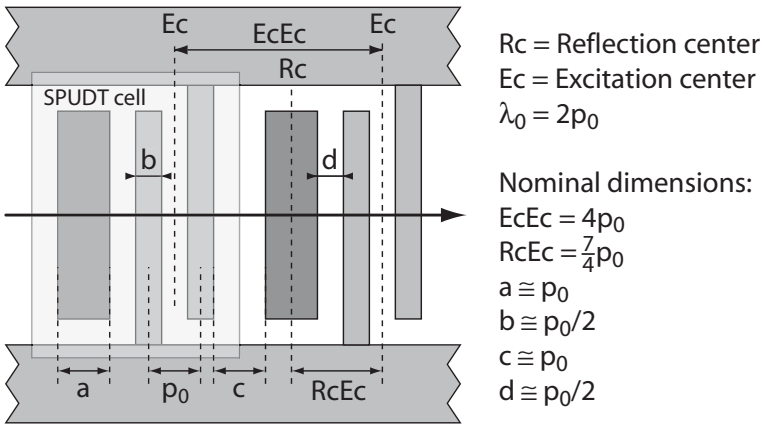


**Figure 4.2**: Parameters of a SPUDT element.

dimensions are thus beyond the large-scale fabrication techniques. To increase the critical dimensions, various grouping schemes [203,217,218], harmonic operation [211, 219], and waveguide coupling of two acoustic tracks supporting different modes [220] have been proposed. In this Thesis, novel SPUDT configurations having the smallest dimension on the order of $\lambda/4$ are introduced [VI,VII]. The directivity of the structure proposed originates from the observed significant difference in the reflectivity of the $\lambda/4$-wide short-circuited electrodes and that of the $\lambda/2$-wide floating electrode on the 128° $LiNbO_3$ substrate [II].

The basic structure of the novel SPUDT configuration is presented in Fig. 4.2. The unit cell is $2\lambda_0$ wide and it consists of a pair of $0.2\lambda_0$-wide transducer electrodes ($b/p_0 = 0.4$) and a single floating $0.4\lambda_0$-wide (second-harmonic operation: $a/\lambda_0 = 0.4$) reflector electrode. The optimal unit cell geometry maximizing the directivity was confirmed via FEM/BEM simulations [148, 149] where the offset of the reflector electrode from the nominal position was varied. Within the unit cell, the center of excitation of surface waves lies in the middle of the gap between the transducer electrodes, and the center of reflection is located in the middle of the reflector electrode. The wide reflector electrode replaces another pair of transducer electrodes present in a synchronous IDT structure. The center of the reflecting electrode is shifted a distance $\lambda_0/8$ away from the synchronous position of the center of the (withdrawn) transducer electrode adjacent to the remaining pair of transducer electrodes. In such an arrangement, waves reflected in the forward direction (towards right in Fig. 4.2) interfere constructively while those propagating in the backward direction tend to cancel each other. The unidirectional operation is obtained with the critical dimension $0.2\lambda_0$, a value typical in normal bidirectional IDTs. On the 128° $LiNbO_3$ substrate at the frequency 2.5 GHz, this dimension corresponds to roughly 325 nm, which is accessible for standard optical lithography.

Other SPUDT configurations based on the basic structure of Fig. 4.2 are possible. A topology where a single wide floating electrode is replaced by several $\lambda_0/2$-spaced floating electrodes may be considered. Then, if the minimum critical dimension of

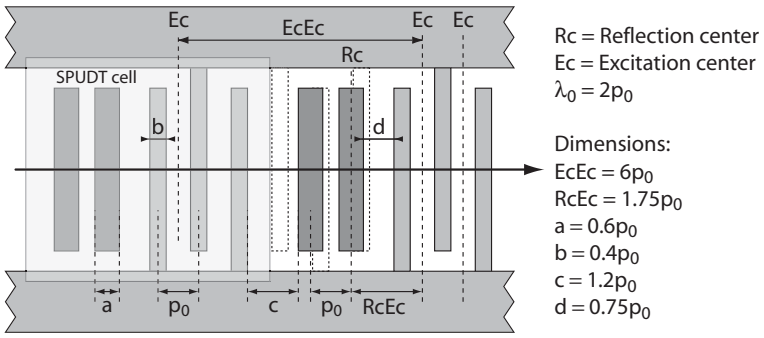


**Figure 4.3**: The $3\lambda_0$-wide unit cell consists of two floating reflector electrodes ($a/p_0 = 0.6$) and three narrow transducer electrodes ($b/p_0 = 0.4$). The dashed rectangles indicate the positions of transducer fingers in a synchronous structure.

$0.2\lambda_0$ is to be maintained, the maximum metallisation ratio allowed for the floating electrodes is 0.6. In addition, the length of a unit cell has to be longer. For example, a unit cell consisting of two $\lambda_0/2$-spaced floating electrodes and three transducer electrodes would occupy 3 wavelengths, see Fig. 4.3. This and longer variants of the SPUDT unit cell structure may be considered to belong to the reflector bank structure introduced by Lewis [203].

## 4.4 Performance of novel SPUDT filters

The SPUDT transducer should combine a wide bandwidth with low losses. Losses can be minimized by maximizing the SPUDT directivity via increasing the length of the device. However, a long transducer implies a narrow frequency bandwidth. Thus, a compromize allowing losses larger than the obtainable minimum while requiring a sufficient bandwidth is pursued. The properties of a delay line consisting of two identical SPUDTs having 9 unit cell sections of Fig. 4.2, with their forward directions opposite to each other, were studied. The numerical simulation of the transmission response for the device is shown in Fig. 4.4. Using lossless Green's functions for the substrate and ignoring the resistivity of the electrodes, an insertion loss of roughly 3 dB at the center frequency of 2.415 GHz and a 100-MHz bandwidth are predicted for the SPUDT filter in the matched condition. The loss level may be attributed to the finite directivity of the transducers. Since multiple-transit signals are necessarily present in the delay line response, the time-gating technique described in Sec. 2.2 is used to facilitate the determination of the insertion loss and the 3 dB bandwidth.

The impedance matching affects the performance of an electric device. If the characteristic impedance of the device differs from that of the impedance environment, part of the energy transmitted through the device is reflected back due to the electrical mismatch, instead of being delivered to the load. In the case of the SPUDT filter configurations referred to in Sec. 4.3, with the period $p_0 = 0.8$ $\mu$m and a 75 $\mu$m aperture, the characteristic impedance is on the order of 350 $\Omega$, a value differing

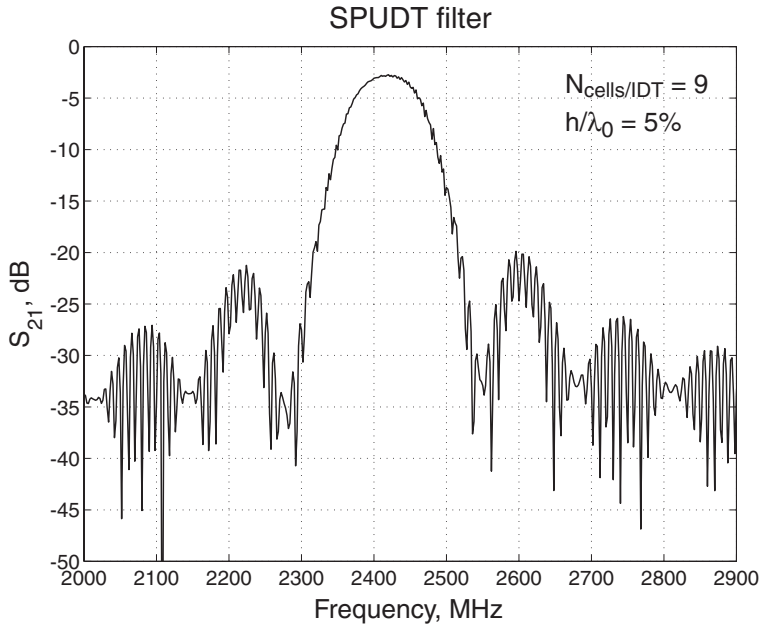


**Figure 4.4**: Simulated frequency response of a matched SPUDT transversal filter. Here, $h/\lambda_0 = 5\%$ and for both transducers, $\mathrm{N_{cells/IDT}} = 9$.

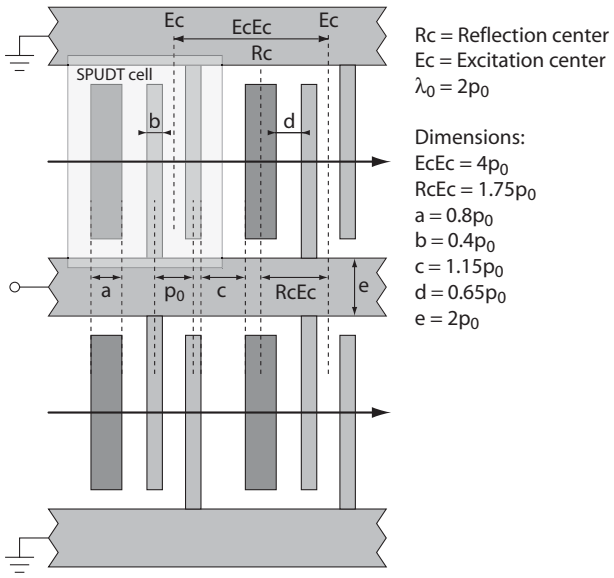


**Figure 4.5**: Double-aperture variant of the SPUDT structure in Fig. 4.2.

significantly from the conventional 50 Ω design and measurement environment. A simple way of reducing the characteristic impedance to one half is to use two parallel signal paths. In practice, this is easily accomplished by implementing two parallel acoustic channels with common input and output, see Fig. 4.5.

The experimental results reveal the presence of loss mechanisms, see Fig. 4.6. The

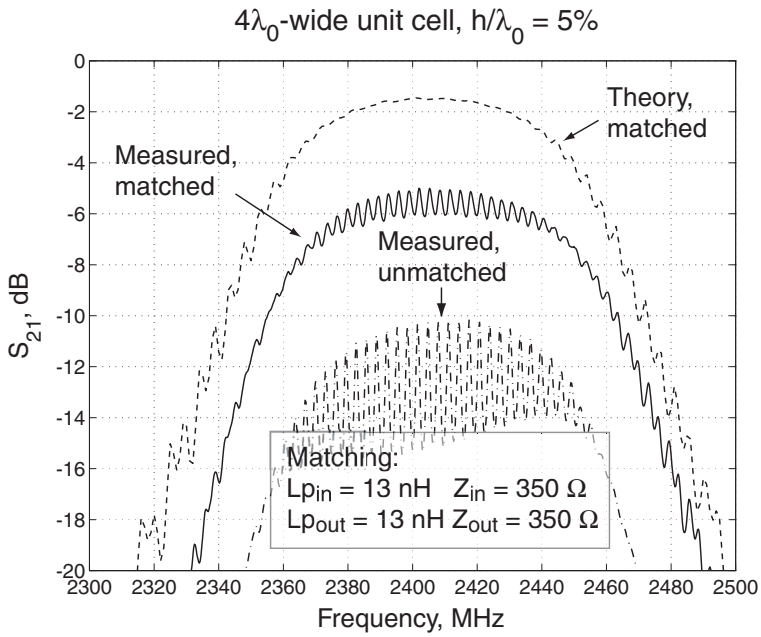


**Figure 4.6**: Comparison of simulated and experimental frequency responses of a transversal SPUDT filter. For both transducers, the unit cell is $4\lambda_0$ wide with four transducer electrodes and three reflecting floating electrodes. Here, $N_{\text{cells/IDT}} = 5$.

difference of the matched experimental and matched simulated results may be largely attributed to the intrinsic attenuation on the free surface, the attenuation inside the electrode structure and the resistivity of the electrodes. However, the estimations made in Paper VII suggest that loss mechanisms not accounted for further degrade the device performance.

# 5 Discussion

This Thesis focuses on the analysis and application of reflecting structures for SAW devices on 128° Y-cut $LiNbO_3$. The accomplishments of the present research are the additional elements introduced to the data analysis tools already available in the SAW research, their efficient use to extract quantitative data on the various structures of interest and the implementation of innovative SAW devices based on the parameters extracted. In this Thesis, the feasibility of a number of data analysis methods is demonstrated and a large amount of values for design parameters, dependent on the electrode geometry, are presented. The results provide a data basis for different designs, setting a good initial value for optimization.

Even though fairly reliable parameter values are achieved, challenges still remain in the roadmap towards more accurate characterization. Possible inaccuracies originate from the implementation of the numerical operations in the simulation software, from errors arising from the time gating procedure used in the analysis, and from the phenomenological nature of the model employed as the framework for the parameters. As far as the performance of the simulation tool is concerned, the numerical results obtained may be compared to experiments to study and enhance the accuracy.

The reflectivity of long structures on various combinations of metal electrodes on a piezoelectrical substrate has been studied extensively in the literature using simulators for infinite periodic arrays. The finiteness of the structures in actual devices gives rise to behaviour which is not necessarily predicted by the infinite periodic models. In order to test the accuracy of simulations of infinite arrays, simulations of finite structures are carried out. In this Thesis, the properties of reflector gratings operating at the second harmonic frequency, as well as those of short structures are studied. Several methods are proposed for the extraction of the reflectivity, and the results are given in the framework of the COM model. An unexpectedly high reflectivity is found for gratings operating at the second harmonic frequency, which, together with the low spurious level of 128° $LiNbO_3$, is favourable for a number of applications. Short reflectors for which the end effects are pronounced are shown to exhibit properties different from those of a unit section in an infinite array. The energy scattered from short reflectors, compared to the energy reflected back as a SAW, is estimated to be a significant contribution — in many cases, the scattering is the dominant phenomenon. The phases of the reflection and transmission coefficients of short reflectors are studied as functions of the cross-sectional profile of the electrode. For the first time, extensive quantitative data is presented, providing a solid basis for a designer.

The evaluation of attenuation inside a reflector grating is a problem difficult to address. The propagation attenuation on a free or metallized surface may be evaluated fairly accurately by simple delay line experiments but estimating the scattering of the SAW signal incident on a grating is a more challenging task to tackle. The effects of reflectivity and attenuation manifest themselves in a similar manner in the

frequency response of the reflector and, in most practical cases, the reflectivity is the dominant phenomenon. In this Thesis, explicit means to evaluate the attenuation inside a reflector grating are presented. A simple method proposed allows one to directly evaluate the attenuation from the level of the minima of the reflection response normalized by the transmission characteristics of the grating. Furthermore, carrying out numerical simulations in which the propagation losses are excluded, an extraction method is provided for estimating losses due to the scattering only. To the best knowledge of the author, the results obtained here constitute the first set of data for attenuation inside gratings as a function of the electrode geometry. Although the attenuation results are ample for the substrate studied, there are questions which remain unanswered. To mention one topic, a particular issue possibly resolvable using the methods used in this work is the frequency dependence of the attenuation parameter.

The topics discussed in this Thesis are relevant for practical device designs, foremost in the field of SAW passive RF interrogation. SAW ID tags comprise an IDT and a number of different reflectors, both being elements studied in this work. Moreover, a compromise between the tag size, the resolution of the manufacturing technology and the available frequency band for the system should be made. In this work, an innovation was introduced, allowing the high-volume fabrication of a low-loss SAW transducer for operation in the 2.45 GHz ISM band. The foundation of this improvement lies in the observed significant difference in the reflectivities of wide floating and narrow grounded electrodes, which may be exploited to achieve unidirectional operation of an IDT.

A recently proposed novel scheme [221,222] overcomes the drawback of the earlier SAW tag systems. Despite the good technical performance of the latter, the limitation on the number of different codes available hindered the widespread commercial use of SAW tags. In the proposed new scheme, the data capacity is foreseen to be sufficient for a global system, a feature necessary to challenge the currently used bar code system. Using the proposed technique, the number of unique tag numbers available is reported to exceed $10^{15}$ [221]. A variety of short reflectors is needed for encoding the input signal. A successful implementation of the system requires precise knowledge of the reflection, transmission and loss characteristics of each individual reflector.

This system is envisaged to monitor the phases of the partial reflected signals, in addition to their amplitudes. Parallel with the study of small-signal amplitudes, the analysis of their phases constitutes an independent contribution in the present work. Here, for the first time, quantitative data for the phase changes associated with the reflection from and transmission through short SAW reflector gratings is provided. However, the results obtained are to be considered as preliminary in nature until supportive findings in parallel topics serve to confirm them.

The future developments in SAW identification will show whether the results of this work will have an impact beyond the scientific community of acoustical signal processing.

# References


[1] Lord Rayleigh,"On waves propagated along the plane surface of an elastic solid", *Proc. London Math. Society*, Vol. 17, 12 Nov 1885, pp. 4–11.

[2] J. Curie and P. Curie, "Développement par pression, de l'électricité polaire dans les cristaux hémièdres à faces inclinées", *Comptes Rendus*, Vol. 91, 1880, p. 294.

[3] R. M. White and F. W. Voltmer, "Direct piezoelectric coupling to surface elastic waves", *Appl. Phys. Lett.*, Vol. 7, No. 12, 15 Dec 1965, pp. 314–316.

[4] C. Tseng and R. M. White, "Propagation of piezoelectric and elastic surface waves on the basal plane of hexagonal piezoelectric crystals", *J. Appl. Phys.*, Vol. 38, No. 11, October 1967, pp. 4274–4280; C. Tseng, "Elastic surface waves on free surface and metallised surface of CdS, ZnO, and PZT-4", *J. Appl. Phys.*, Vol. 38, No. 11, October 1967, pp. 4281–4284.

[5] H. Engan, K. A. Ingebrigtsen, and A. Tonning, "Elastic surface waves in $\alpha$-quartz: Observation of leaky surface waves", *Appl. Phys. Lett.*, Vol. 10, No. 11, 1 June 1967, pp. 311–313.

[6] T. C. Lim and G. W. Farnell, "Search for forbidden directions of elastic surface-wave propagation in anisotropic crystals", *J. Appl. Phys.*, Vol. 39, No. 9, August 1968, pp. 4319–4325.

[7] T. C. Lim and G. W. Farnell, "Character of pseudo surface waves on anisotropic crystals", *J. Acoust. Soc. Am.*, Vol. 45, No. 4, April 1969, pp. 845–851.

[8] N. E. Glass and A. A. Maradudin, "Leaky surface-elastic waves on both flat and strongly corrugated surfaces for isotropic, nondissipative media", *J. Appl. Phys.*, Vol. 54, No. 2, February 1983, pp. 796–805.

[9] S. Tonami, A. Nishikata, and Y. Shimizu, "Characteristics of leaky surface acoustic waves propagating on $LiNbO_3$ and $LiTaO_3$ substrates", *Japan. J. Appl. Phys.*, Vol. 34, Part 1, No. 5B, May 1995, pp. 2664–2667.

[10] J. Bleustein, "A new surface wave in piezoelectric materials", *Appl. Phys. Lett.*, Vol. 13, No. 12, 15 December 1968, pp. 412–413.

[11] Yu. V. Gulyaev, "Electroacoustic surface waves in solids", *Zh. Eksp. Teor. Fiz., Pis. Red.*, Vol. 9, No. 1, 5 January 1969, pp. 63–65; English translation: *JETP Lett.*, Vol. 9, No. 1, 5 January 1969, pp. 37–38.

[12] J. Götz, "Über den Schalldurchgang durch Metallplatten in Flüssigkeiten bei schrägem Einfall einer ebenen Welle", *Akustische Zeitschrift*, Vol. 8, No. 5, October 1943, pp. 145–168.

[13] W. P. Mason, "Quartz crystal applications", *Bell System Tech. J.*, Vol. 22, No. 2, July 1943, pp. 178–220.

[14] W. G. Cady, "Piezoelectricity", McGraw–Hill, New York, 1946, 806 p.

[15] W. P. Mason, "Piezoelectric crystals and their application to ultrasonics", Van Nostrand, New York, 1950, 508 p.

[16] N. Wooster and W. A. Wooster, "Preparation of synthetic quartz", *Nature*, Vol. 157, No. 3984, 9 March 1946, p. 297.

[17] D. R. Hale, "Laboratory growing of quartz", *Science*, Vol. 107, No. 2781, 16 April 1948, pp. 393–394.

[18] E. Buehler and A. C. Walker, "Growing quartz crystals", *Sci. Monthly*, Vol. 69, No. 9, September 1949, pp. 148–155.

[19] A. C. Walker and E. Buehler, "Growing large quartz crystals", *Ind. Eng. Chem.*, Vol. 42, No. 7, July 1950, pp. 1369–1375.

[20] C. S. Brown, R. C. Kell, L. A. Thomas, N. Wooster, and W. A. Wooster, "Growth of large quartz crystals", *Nature*, Vol. 167, No. 4258, 9 June 1951, 940–941.

[21] A. C. Walker, "Hydrothermal synthesis of quartz crystals", *J. Am. Ceram. Soc.*, Vol. 36, No. 8, August 1953, pp. 250–256.

[22] A. C. Walker, "Hydrothermal growth of quartz crystals as related to phase considerations", *Ind. Eng. Chem.*, Vol. 46, No. 8, August 1954, pp. 1670–1676.

[23] H. Jaffe and D. A. Berlincourt, "Piezoelectric transducer materials", *Proc. IEEE*, Vol. 53, No. 10, October 1965, pp. 1372–1386.

[24] F. R. Lack, G. W. Willard, and I. E. Fair, "Some improvements in quartz crystal circuit elements", *Bell System Tech. J.*, Vol. 13, No. 3, July 1934, pp. 453–463.

[25] W. P. Mason, "Zero temperature coefficient quartz crystals for very high temperatures", *Bell System Tech. J.*, Vol. 30, No. 2, April 1951, pp. 366–380.

[26] H. E. Bömmel, W. P. Mason, and A. W. Warner, Jr., "Experimental evidence for dislocations in crystalline quartz", *Phys. Rev.*, Vol. 99, No. 6, 15 September 1955, pp. 1894–1896.

[27] H. E. Bömmel, W. P. Mason, and A. W. Warner, Jr., "Dislocations, relaxations and anelasticity of crystal quartz", *Phys. Rev.*, Vol. 102, No. 1, 1 April 1956, pp. 64–71.

[28] H. Deresiewicz and R. D. Mindlin, "Waves on the surface of a crystal", *J. Appl. Phys.*, Vol. 28, No. 6, June 1957, pp. 669–671.

[29] R. Bechmann, "Elastic and piezoelectric constants of alpha-quartz", *Phys. Rev.*, Vol. 110, No. 5, 1 June 1958, pp. 1060–1061.

[30] K. A. Ingebrigtsen and A. Tonning, "Numerical data for acoustic surface waves in $\alpha$-quartz and cadmium sulfide", *Appl. Phys. Lett.*, Vol. 9, No. 1, 1 July 1966, pp. 16–18.

[31] G. A. Coquin and H. F. Tiersten, "Analysis of the excitation and detection of piezoelectric surface waves in quartz by means of surface electrodes", *J. Acoust. Soc. Am.*, Vol. 41, Part 2, No. 4, April 1967, pp. 921–939.

[32] E. Salzmann, T. Plieninger, and K. Dransfeld, "Attenuation of elastic surface waves in quartz at frequencies of 316 MHz and 1047 MHz", *Appl. Phys. Lett.*, Vol. 13, No. 1, 1 July 1968, pp. 14–15.

[33] M. R. Daniel and J. de Klerk, "Temperature-dependent attenuation of ultrasonic surface waves in quartz", *Appl. Phys. Lett.*, Vol. 16, No. 1, 1 January 1970, pp. 30–31.

[34] B. T. Matthias and J. P. Remeika, "Ferroelectricity in the ilmenite structure", *Phys. Rev.*, Vol. 76, No. 12, 15 December 1949, pp. 1886–1887.

[35] A. A. Ballman, "Growth of piezoelectric and ferroelectric materials by the Czochralski technique", *J. Am. Ceram. Soc.*, Vol. 48, No. 2, February 1965, pp. 112–113.

[36] A. W. Warner, "New piezoelectric materials", *Proc. IEEE 19$^{th}$ Freq. Contr. Symp.*, 20–22 May 1965, pp. 5–21.

[37] K. Nassau and H. J. Levinstein, "Ferroelectric behavior of lithium niobate", *Appl. Phys. Lett.*, Vol. 7, No. 3, 1 August 1965, pp. 69–70.

[38] C. P. Wen and R. F. Mayo, "Acoustic attenuation of a single-domain lithium niobate crystal at microwave frequencies", *Appl. Phys. Lett.*, Vol. 9, No. 4, 15 August 1966, pp. 135–136.

[39] T. Yamada, N. Niizeki, and H. Toyoda, "Piezoelectric and elastic properties of lithium niobate single crystals", *Japan. J. Appl. Phys.*, Vol. 6, No. 2, February 1967, pp. 151–155.

[40] A. B. Smith, M. Kestigian, R. W. Kedzie, and and I. M. Grace, "Shear-wave attenuation in lithium niobate", *J. Appl. Phys.*, Vol. 38, No. 12, November 1967, pp. 4928–4929.

[41] A. W. Warner, M. Onoe, and G. A. Coquin, "Determination of elastic and piezoelectric constants for crystals in class (3m)", *J. Acoust. Soc. Am.*, Vol. 42, No. 6, December 1967, pp. 1223–1231.

[42] E. G. Spencer, P. V. Lenzo, and A. A. Ballman, "Dielectric materials for electrooptic, elastooptic, and ultrasonic device applications", *Proc. IEEE*, Vol. 55, No. 12, December 1965, pp. 2074–2108.

[43] F. W. Voltmer, E. P. Ippen, and R. M. White, "Measured and calculated surface-wave velocities", *Proc. IEEE*, Vol. 56, No. 9, September 1968, pp. 1634–1635.

[44] A. J. Slobodnik, Jr., "Microwave frequency acoustic surface wave propagation losses in $LiNbO_3$", *Appl. Phys. Lett.*, Vol. 14, No. 3, 1 February 1969, pp. 94–96.

[45] A. P. Korolyuk, L. Ya. Matsakov, and V. V. Vasil'chenko, "Determination of elastic and piezoelectric constants of lithium niobate single crystals", *Kristallografija / Akademija nauk*, Vol. 15, No. 5, September–October 1970, pp. 1028–1032; English translation: *Soviet Physics – Crystallography*, Vol. 15, No. 5, March–April 1971, pp. 893–896.

[46] R. T. Smith and F. S. Welsh, "Temperature dependence of the elastic, piezoelectric, and dielectric constants of lithium tantalate and lithium niobate", *J. Appl. Phys.*, Vol. 42, No. 6, May 1971, pp. 2219–2230.

[47] Y. Nakagawa, K. Yamanouchi, and K. Shibayama, "Third-order elastic constants of lithium niobate", *J. Appl. Phys.*, Vol. 44, No. 9, September 1973, pp. 3969–3974.

[48] R. A. Graham, "Second- and third-order piezoelectric stress constants of lithium niobate as determined by the impact-loading technique", *J. Appl. Phys.*, Vol. 48, No. 6, June 1977, pp. 2153–2163.

[49] G. Kovacs, M. Anhorn, H. E. Engan, G. Visintini, and C. C. W. Ruppel, "Improved material constants for $LiNbO_3$ and $LiTaO_3$", *Proc. 1990 IEEE Ultrason. Symp.*, pp. 435–438.

[50] J. Kushibiki, I. Takanaga, M. Arakawa, and T. Sannomiya, "Accurate measurements of the acoustical physical constants of $LiNbO_3$ and $LiTaO_3$ single crystals", *IEEE Trans. Ultrason., Ferroelectr., Freq. Contr.*, Vol. 46, No. 5, September 1999, pp. 1315–1323.

[51] P. V. Lenzo, E. H. Turner, E. G. Spencer, and A. A. Ballman, "Electrooptic coefficients and elastic-wave propagation in single-domain ferroelectric lithium tantalate", *Appl. Phys. Lett.*, Vol. 8, No. 4, 15 February 1966, pp. 81–82.

[52] H. J. Levinstein, A. A. Ballman, and C. D. Capio, "Domain structure and Curie temperature of single-crystal lithium tantalate", *J. Appl. Phys.*, Vol. 37, No. 12, November 1966, pp. 4585–4586.

[53] R. T. Smith, "Elastic, piezoelectric and dielectric properties of lithium tantalate", *Appl. Phys. Lett.*, Vol. 11, No. 5, 1 September 1967, pp. 146–148.

[54] T. Yamada, H. Iwasaki, and N. Niizeki, "Piezoelectric and elastic properties of $LiTaO_3$ temperature characteristics", *Japan. J. Appl. Phys.*, Vol. 8, No. 9, September 1969, pp. 1127–1132.

[55] J. J. Campbell and W. R. Jones, "A method for estimating optimal crystal cuts and propagation directions for excitation of piezoelectric surface waves", *IEEE Trans. Son. Ultrason.*, Vol. SU-15, No. 4, October 1968, pp. 209–217.

[56] K. Nakamura, M. Kazumi, and H. Shimizu, "SH-type and Rayleigh-type surface waves on rotated Y-cut $LiTaO_3$", *Proc. 1977 IEEE Ultrason. Symp.*, pp. 819–822.

[57] O. Kawachi, G. Endoh, M. Ueda, O. Ikata, K. Hashimoto, and M. Yamaguchi, "Optimum cut of $LiTaO_3$ for high performance leaky surface acoustic wave filters", *Proc. 1996 IEEE Ultrason. Symp.*, pp. 71–76.

[58] A. J. Slobodnik, Jr. and E. D. Conway, "New high-frequency high-coupling low-beam-steering cut for acoustic surface waves on $LiNbO_3$", *Electr. Lett.*, Vol. 6, No. 6, 19 March 1970, pp. 171–173.

[59] A. Takanayagi, K. Yamanouchi, and K. Shibayama, "Piezoelectric leaky surface wave in $LiNbO_3$", *Appl. Phys. Lett.*, Vol. 17, No. 5, 1 September 1970, pp. 225–227.

[60] K. Yamanouchi and K. Shibayama, "Propagation and amplification of Rayleigh waves and piezoelectric leaky surface waves in $LiNbO_3$", *J. Appl. Phys.*, Vol. 43, No. 3, March 1972, pp. 856–862.

[61] K. Shibayama and K. Yamanouchi, "Optimum cut for rotated Y-cut $LiNbO_3$ crystal used as the substrate of acoustic-surface-wave filters", *Proc. IEEE*, Vol. 64, No. 5, May 1976, pp. 595–597.

[62] Ref. [15], p. 208.

[63] Z. Chang and G. R. Barsch, "Elastic constants and thermal expansion of berlinite", *IEEE Trans. Son. Ultrason.*, Vol. SU-23, No. 2, March 1976, pp. 127–135.

[64] A. Ballato and G. J. Iafrate, "The angular dependence of piezoelectric plate frequencies and their temperature coefficients", *Proc. $30^{th}$ IEEE Freq. Contr. Symp.*, 2–4 June 1976, pp. 141–156.

[65] E. D. Kolb and R. A. Laudise, "Hydrothermal synthesis of aluminum orthophosphate", *J. Cryst. Growth*, Vol. 43, No. 3, April 1978, pp. 313–319.

[66] H. Poignant, L. le Marechal, and Y. Toudic, "Etude de la solubilité du phosphate d'aluminium ($AlPO_4$) dans des solutions hydrothermales d'acide orthophosphorique $H_3PO_4$", *Mat. Res. Bull.*, Vol. 14, No. 5, May 1979, pp. 603–612.

[67] D. S. Bailey, J. C. Andle, D. L. Lee, W. Soluch, and J. F. Vetelino, "Temperature dependence of the material and acoustic wave parameters of berlinite", *Proc. 1983 IEEE Ultrason. Symp.*, pp. 335–340.

[68] J. Détaint, A. Zarka, B. Capelle, Y. Toudic, J. Schwarzel, E. Philippot, J. C. Jumas, A. Goiffon, and J. C. Doukhan, "Berlinite: characterization of crystals with a low water concentration and design of bulk wave resonators", *Proc. $40^{th}$ IEEE Freq. Contr. Symp.*, 28–30 May 1986, pp. 101–114.

[69] J. Détaint, J. Schwarzel, A. Zarka, B. Capelle, D. Cochet-Muchy, and E. Philippot, "Properties of the plane and plano-convexe resonators using berlinite, gallium phosphate and langasite", *Proc. 1994 IEEE Ultrason. Symp.*, pp. 1051–1056.

[70] M. P. da Cunha and S. de A. Fagundes, "Investigation on recent quartz-like materials for SAW applications", *IEEE Trans. Ultrason., Ferroelectr., Freq. Contr.*, Vol. 46, No. 6, November 1999, pp. 1583–1590; M. P. da Cunha and S. de A. Fagundes, "Investigation on recent quartz like materials for SAW applications", *Proc. 1998 IEEE Ultrason. Symp.*, pp. 283–288.

[71] W. Wallnöfer, P. W. Krempl, and A. Asenbaum, "Determination of the elastic and photoelastic constants of quartz-type $GaPO_4$ by Brillouin scattering", *Phys. Rev. B*, Vol. 49, No. 15, 15 April 1994, pp. 10075–10080.

[72] J. Détaint, A. Zarka, B. Capelle, D. Palmier, and E. Philippot, "Optimisation of the design of the resonators using the new materials: Application to gallium phosphate and langasite", *Proc. 51$^{st}$ Freq. Contr. Symp.*, 28–30 May 1997, pp. 566–578.

[73] E. H. Briot, E. Bigler, W. Daniau, G. Marianneau, and A. Pakfar, "A comprehensive mapping of surface acoustic wave properties on gallium ortophosphate ($GaPO_4$)", *Proc. Joint Meeting of the European Frequency and Time Forum and The IEEE International Frequency Control Symposium*, 13–16 April 1999, pp. 811–815.

[74] M. P. da Cunha, T. B. Pollard, H. Whitehouse, and P. M. Worsch, "$GaPO_4$ SAW devices: Measured and predicted propagation properties", *Proc. 2003 Ultrason. Symp.*, pp. 110–113.

[75] M. Onoe, A. W. Warner, and A. A. Ballman, "Elastic and piezoelectric characteristics of bismuth germanium oxide $Bi_{12}GeO_{20}$", *IEEE Trans. Son. Ultrason.*, Vol. SU-14, No. 4, October 1967, pp. 165–167.

[76] N. M. Shorrocks, R. M. Whatmore, F. W. Ainger, and I. M. Young, "Lithium tetraborate – a new temperature compensated piezoelectric substrate material for surface acoustic wave devices", *Proc. 1981 IEEE Ultrason. Symp.*, pp. 337–340.

[77] C. D. J. Emin and J. F. Werner, "The bulk acoustic wave properties of lithium tetraborate", *Proc. 37th Freq. Contr. Symp.*, 1–3 June 1983, pp. 136–143.

[78] M. Adachi, T. Shiosaki, H. Kobayashi, O. Ohnishi, and A. Kawabata, "Temperature compensated piezoelectric lithium tetraborate crystal for high frequency surface acoustic wave and bulk acoustic wave applications", *Proc. 1985 IEEE Ultrason. Symp.*, pp. 228–232.

[79] A. A. Kaminskii, I. M. Silvestrova, S. E. Sarkisov, and G. A. Denisenko, "Investigation of trigonal $(La_{1-x}Nd_x)_3Ga_5SiO_{14}$ crystals; II. Spectral laser and electromechanical properties", *Phys. Stat. Sol. (a)*, Vol. 80, No. 2, December 1983, pp. 607–620.

[80] I. M. Silvestrova, Yu. V. Pisarevskii, P. A. Senyushchenkov, and A. I. Krupnyi, "Temperature dependences of the elastic properties of $La_3Ga_5SiO_{14}$ single crystals", *Fiz. Tverd. Tela*, Vol. 28, No. 9, September 1986, pp. 2875–2878; English translation: *Sov. Phys. Solid State*, Vol. 28, No. 9, September 1986, pp. 1613–1614.

[81] V. B. Grouzinenko and V. V. Bezdelkin, "Piezoelectric resonators from $La_3Ga_5SiO_{14}$ (langasite) – single crystals", *Proc. 1992 IEEE Freq. Contr. Symp.*, pp. 707–712.

[82] A. B. Ilyev, B. S. Umarov, L. A. Shabanova, and M. F. Dubovik, "Temperature depencende of electromechanical properties of LGS crystals", *Phys. Stat. Sol. (a)*, Vol. 98, No. 2, December 1986, pp. K109–K114.

[83] K. S. Aleksandrov, B. P. Sorokin, P. P. Turchin, and D. A. Glushkov, "Non-linear piezoelectricity in $La_3Ga_5SiO_{14}$ piezoelectric single crystal", *Ferroelectr. Lett.*, Vol. 14, No. 5–6, September–October 1992, pp. 115–125.

[84] I. M. Silvestrova, V. V. Bezdelkin, P. A. Senyushenkov, and Yu. V. Pisarevsky, "Present stage of $La_3Ga_5SiO_{14}$ – research", *Proc. 1993 IEEE Freq. Contr. Symp.*, pp. 348–350; I. M. Silvestrova, Yu. V. Pisarevsky, V. V. Bezdelkin, and P. A. Senyushenkov, "New piezoelectric materials", *Proc. 1993 IEEE Freq. Contr. Symp.*, pp. 351–352.

[85] S. Sakharov, P. Senyushenkov, A. Medvedev, and Yu. Pisarevsky, "New data on temperature stability and acoustical losses of langasite crystals", *Proc. 1995 IEEE Freq. Contr. Symp.*, pp. 647–652.

[86] S. Sorokin, P. P. Turchin, S. I. Burkov, D. A. Glushkov, and K. S. Aleksandrov, "Influence of static electric field, mechanical pressure, and temperature on the propagation of acoustic waves in $La_3Ga_5SiO_{14}$ piezoelectric single crystals", *Proc. 1996 IEEE Freq. Contr. Symp.*, pp. 161–169.

[87] K. Inoue and K. Sato, "Propagation characteristics of surface acoustic waves on langasite", *Japan. J. Appl. Phys.*, Vol. 37, Part 1, No. 5B, May 1998, pp. 2909–2913.

[88] A. Bungo, C. Jian, K. Yamaguchi, Y. Sawada, S. Uda, and Yu. P. Pisarevsky, "Analysis of surface acoustic wave properties of the rotated Y-cut langasite substrate", *Japan. J. Appl. Phys.*, Vol. 38, Part 1, No. 5B, May 1999, pp. 3239–3243; A. Bungo, C. Jian, K. Yamaguchi, Y. Sawada, R. Kimura and S. Uda, "Experimental and theoretical analysis of SAW properties of the langasite substrate with Euler angle (0°,140°,$\varphi$)", *Proc. 1999 IEEE Ultrason. Symp.*, pp. 231–234.

[89] M. Adachi, T. Karaki, and W. Miyamoto, "Surface acoustic wave properties of $La_3Ga_5SiO_{14}$ (LANGASITE) single crystals", *Japan. J. Appl. Phys.*, Vol. 38, Part 1, No. 5B, May 1999, pp. 3283–3287.

[90] J. Bohm, E. Chilla, C. Flannery, H.-J. Fröhlich, T. Hauke, R. B. Heimann, M. Hengst, and U. Straube, "Czochralski growth and characterization of piezoelectric single crystals with langasite structure: $La_3Ga_5SiO_{14}$ (LGS), $La_3Ga_{5.5}Nb_{0.5}O_{14}$ (LGN) and $La_3Ga_{5.5}Ta_{0.5}O_{14}$ (LGT) II. Piezoelectric and elastic properties", *J. Cryst. Growth*, Vol. 216, Issues 1-4, 15 June 2000, pp. 293–298.

[91] D. C. Malocha, M. P. da Cunha, E. Adler, R. C. Smythe, S. Frederick, M. Chou, R. Helmbold, and Y. S. Zhou, "Recent measurements of material constants versus temperature for langatate, langanite, and langasite", *Proc. 54$^{th}$ Freq. Contr. Symp.*, 7–9 June 2000, pp. 200–205; D. C. Malocha, H. François-Saint-Cyr, K. Richardson, and R. Helmbold, "Measurements of LGS, LGN, and LGT thermal coefficients of expansion and density", *IEEE Trans. Ultrason., Ferroelectr., Freq. Contr.*, Vol. 49, No. 3, March 2002, pp. 350–355.

[92] E. Chilla, C. M. Flannery, H.-J. Frölich, and U. Straube, "Elastic properties of langasite-type crystals determined by bulk and surface acoustic waves", *J. Appl. Phys.*, Vol. 90, No. 12, 15 December 2001, pp. 6084–6091; E. Chilla, C. M. Flannery, H.-J. Frölich, J. Bohm, R. B. Heimann, M. Hengst, and U. Straube, "Elastic constants of langasite-type crystals determined by bulk and surface guided acoustic modes", *Proc. 2002 IEEE Ultrason. Symp.*, pp. 377–380.

[93] J. Schreuer, "Elastic and piezoelectric properties of $La_3Ga_5SiO_{14}$ and $La_3Ga_{5.5}Ta_{0.5}O_{14}$: An application of resonant ultrasound technology", *IEEE Trans. Ultrason., Ferroelectr., Freq. Contr.*, Vol. 49, No. 11, November 2002, pp. 1474–1479; J. Schreuer, J. Rupp, C. Thybaut, and J. Stade, "Temperature dependence of elastic, piezoelectric and dielectric properties of $La_3Ga_5SiO_{14}$ and $La_3Ga_{5.5}Ta_{0.5}O_{14}$: An application of resonant ultrasound technology", *Proc. 2002 IEEE Ultrason. Symp.*, pp. 373–376.

[94] I. B. Yakovkin, R. M. Taziev, and A. S. Kozlov, "Numerical and experimental investigation SAW in langasite", *Proc. 1995 IEEE Ultrason. Symp.*, pp. 389–392.

[95] T. Sato, A. Nishikata, and Y. Shimizu, "Characteristics of surface acoustic waves propagating on a $La_3Ga_5SiO_{14}$ substrate", *Japan. J. Appl. Phys.*, Vol. 36, Part 1, No. 5B, May 1997, pp. 3068–3070.

[96] T. Satoh and A. Mori, "Surface acoustics wave propagation characteristics on a langasite crystal plate", *Japan. J. Appl. Phys.*, Vol. 36, Part 1, No. 5B, May 1997, pp. 3071–3073.

[97] V. N. Fedorets, Yu. P. Kondratyev, B. V. Mill, V. A. Pankov, Yu. V. Pisarevsky, and V. V. Timashev, "Surface acoustic wave characteristics on $La_3Ga_5SiO_{14}$ crystals", *Proc. 1997 IEEE Freq. Contr. Symp.*, pp. 816–820.

[98] J. Koskela, S. Lehtonen, V. P. Plessky, and M. M. Salomaa, "Surface transverse waves on langasite", *Appl. Phys. Lett.*, Vol. 72, No. 21, 25 May 1998, pp. 2665–2667; V. P. Plessky, J. Koskela, S. Lehtonen, and M. M. Salomaa, "Surface transverse waves on langasite", *Proc. 1998 IEEE Ultrason. Symp.*, pp. 139–142.

[99] T. Sato, M. Murota, and Y. Shimizu, "Characteristics of Rayleigh and leaky surface acoustic wave propagating on a $La_3Ga_5SiO_{14}$ substrate", *Japan. J. Appl. Phys.*, Vol. 37, Part 1, No. 5B, May 1998, pp. 2914–2917.

[100] M. Takeuchi, M. Tanaka, and Y. Imanishi, "SAW reflection characteristics and NSPUDT orientations on langasite", *Proc. 1998 IEEE Ultrason. Symp.*, pp. 297–300.

[101] K. Inoue and K. Sato, "Temperature stability of SAW on langasite single crystals", *Proc. 1998 IEEE Ultrason. Symp.*, pp. 301–306.

[102] M. Kadota, J. Nakanishi, T. Kitamura, and M. Kumatoriya, "Surface acoustic wave properties on various rotated Y-cut langasite crystal substrates grown by the Czockralski method", *Proc. 1998 IEEE Ultrason. Symp.*, pp. 311–314.

[103] R. C. Smythe, R. C. Helmhold, G. E. Hague, and K. A. Snow, "Langasite, langanite, and langatate resonators: recent results", *Proc. Joint Meeting of the European Frequency and Time Forum and The IEEE International Frequency Control Symposium*, 13–16 April 1999, pp. 816–820.

[104] E. H. Briot, E. Bigler, S. Ballandras, G. Marianneau, and M. Solal, "Experimental measurements of velocities and temperature effects for SAWs on Y-rotated cuts of langasite", *Electr. Lett.*, Vol. 35, No. 20, 30 September 1999, pp. 1780–1782.

[105] N. F. Naumenko and V. S. Orlov, "Optimal cut for SAW devices on langasite", U. S. Patent 5,917,265, 29 June 1999; N. F. Naumenko and L. P. Solie, "Optimal cut of langasite for high performance SAW devices", *Proc. 1999 IEEE Ultrason. Symp.*, pp. 243–248.

[106] V. B. Chvets, P. G. Ivanov, V. M. Makarov, and V. S. Orlov, "Design of SAW filters on langasite", *Proc. 1999 IEEE Ultrason. Symp.*, pp. 295–299.

[107] J. Bohm, R. B. Heimann, M. Hengst, R. Roewer, and J. Schindler, "Czochralski growth and characterization of piezoelectric single crystals with langasite structure: $La_3Ga_5SiO_{14}$ (LGS), $La_3Ga_{5.5}Nb_{0.5}O_{14}$ (LGN) and $La_3Ga_{5.5}Ta_{0.5}O_{14}$ (LGT) Part I", *J. Cryst. Growth*, Vol. 204, Issues 1-2, 1 July 1999, pp. 128–136.

[108] T. Viken, S. Rooth, S. Bardal, E. Halvorsen, Ø. Johansen, and A. Rønnekleiv, "SAW properties of langasite with Euler angles [0°,140°,25°]", *Proc. 2000 IEEE Ultrason. Symp.*, pp. 249–252.

[109] R. Fachberger, E. Riha, E. Born, W. Ruile, U. Wolff, P. Pongratz, and S. Kronholz, "NSPUDT resonator on langasite", *Proc. 2002 IEEE Ultrason. Symp.*, pp. 501–504.

[110] J. Schreuer, C. Thybaut, M. Prestat, J. Stade, and E. Haussühl, "Towards an understanding of the anomalous electromechanical behaviour of langasite and related compounds at high temperatures", *Proc. 2003 IEEE Ultrason. Symp.*, pp. 196–199.

[111] A. A. Kaminskii, B. V. Mill, E. L. Belokoneva, S. E. Sarkisov, T. Yu. Pastukhova, and G. G. Khodzabagyan, "Crystal structure and simulated emission of $La_3Ga_5Nb_{0.5}O_{14}$–$Nd^{3+}$", *Izv. Acad. Nauk SSSR, Neorg. Mat.*, Vol. 20, No. 12, December 1984, pp. 2057–2058; English translation: *Inorg. Mat.*, Vol. 20, No. 12, December 1984, pp. 1793–1796.

[112] I. M. Silvestrova, Yu. V. Pisarevskii, A. A. Kaminskii, and B. V. Mill, "Elastic, piezoelectric, and dielectric properties of $La_3Ga_5Nb_{0.5}O_{14}$ crystals", *Fiz. Tverd. Tela*, Vol. 29, No. 5, May 1987, pp. 1520–1522; English translation: *Sov. Phys. Solid State*, Vol. 29, No. 5, May 1987, pp. 870–871.

[113] Yu. V. Pisarevsky, P. A. Senyushencov, P. A. Popov, and B. V. Mill, "New strong piezoelectric $La_3Ga_5Nb_{0.5}O_{14}$ with temperature compensation cuts", *Proc. 49$^{th}$ Freq. Contr. Symp.*, 29 May – 2 June 1995, pp. 653–656.

[114] A. A. Kaminskii, A. P. Shkaradevich, B. V. Mill, V. G. Koptev, A. V. Butashin, and A. A. Demidovich, "Tunable simulated emission of $Cr^{3+}$ ions and generation frequency self-multiplication effect in acentric crystals of Ca-gallogermanate structure", *Izv. Acad. Nauk SSSR, Neorg. Mat.*, Vol. 24, No. 4, April 1988, pp. 696–692; English translation: *Inorg. Mat.*, Vol. 24, No. 4, April 1988, pp. 579–581.

[115] Yu. V. Pisarevsky, P. A. Senyushenkov, B. V. Mill, and N. A. Moiseeva, "Elastic, piezoelectric, dielectric properties of $La_3Ga_5Ta_{0.5}O_{14}$ single crystals", *Proc. 52nd Freq. Contr. Symp.*, 27–29 May 1998, pp. 742–747.

[116] M. P. da Cunha, E. L. Adler, and D. C. Malocha, "Surface and pseudo surface acoustic waves in langatate", *Proc. 1999 IEEE Ultrason. Symp.*, pp. 169–172.

[117] N. Onozato, M. Adachi, and T. Karaki, "Surface acoustic wave properties of $La_3Ga_5Ta_{0.5}O_{14}$ single crystals", *Japan. J. Appl. Phys.*, Vol. 39, Part 1, No. 5B, May 2000, pp. 3028–3031.

[118] M. P. da Cunha and D. C. Malocha, "Pure shear horizontal SAW on langatate", *Proc. 2000 IEEE Ultrason. Symp.*, pp. 231–234; M. P. da Cunha and D. C. Malocha, "Experimental and predicted SAW temperature behavior of langatate", *Proc. 2000 IEEE Ultrason. Symp.*, pp. 245–248.

[119] M. P. da Cunha, D. C. Malocha, D. Puccio, J. Thiele, and T. Pollard, "High coupling, zero TCD SH wave on LGX", *Proc. 2002 IEEE Ultrason. Symp.*, pp. 381–384.

[120] W. L. Johnson, S. A. Kim, D. S. Lauria, and R. C. Smythe, "Acoustic damping in langatate as a function of temperature, frequency, and mechanical contact", *Proc. 2002 IEEE Ultrason. Symp.*, pp. 961–964.

[121] K. Yamanouchi, H. Odagawa, T. Kojima, and T. Matsumura, "Theoretical and experimental study of super-high electromechanical coupling surface acoustic wave propagation in $KNbO_3$ single crystal", *Electr. Lett.*, Vol. 33, No. 3, 30 January 1997, pp. 193–194; H. Odagawa, T. Matsumura, and K. Yamanouchi, "Super high electromechanical coupling and zero-temperature characteristics of $KNbO_3$ and its applications for low-loss wide band filters", *Proc. 1997 IEEE Ultrason. Symp.*, pp. 235–238; K. Yamanouchi and H. Odagawa, "Super high electromechanical coupling and zero temperature coefficient surface acoustic wave substrates in $KNbO_3$ single crystal", *IEEE Trans. Ultrason., Ferroelectr., Freq. Contr.*, Vol. 46, No. 3, May 1999, pp. 700–705.

[122] M. Zgonik, R. Schlesser, I. Biaggio, E. Voit, J. Tscherry, and P. Günter, "Materials constants of $KNbO_3$ relevant for electro- and acoustic-optics", *J. Appl. Phys.*, Vol. 74, No. 2, 15 July 1993, pp. 1287–1297.

[123] K. Nakamura and M. Oshiki, "Theoretical analysis of horizontal shear mode piezoelectric surface acoustic waves in potassium niobate", *Appl. Phys. Lett.*, Vol. 71, No. 22, 1 December 1997, pp. 3203–3205; K. Nakamura, M. Oshiki, and H. Kitazume, "SH-mode SAW and its acousto-optic interaction in $KNbO_3$", *Proc. 1998 IEEE Ultrason. Symp.*, pp. 1305–1308.

[124] K. Nakamura and Y. Kawamura, "Orientation dependence of electromechanical coupling factors in $KNbO_3$", *IEEE Trans. Ultrason., Ferroelectr., Freq. Contr.*, Vol. 47, No. 3, May 2000, pp. 750–755; K. Nakamura and Y. Kawamura, "Electromechanical coupling factor of $KNbO_3$ single crystal", *Proc. 1999 IEEE Ultrason. Symp.*, pp. 1013–1018.

[125] C. Zhang, J. J. Caron, and J. F. Vetelino, "The Bleustein-Gulyaev wave mode in potassium niobate for liquid sensing applications", *Proc. 2000 IEEE Ultrason. Symp.*, pp. 263–268.

[126] V. G. Mozhaev and M. Weihnacht, "Sectors of nonexistence of surface acoustic waves in potassium niobate", *Proc. 2002 IEEE Ultrason. Symp.*, pp. 391–395.

[127] T. B. Pollard, J. F. Vetelino, and M. P. da Cunha, "Pure SH SAW on single crystal $KNbO_3$ for liquid sensor applications", *Proc. 2003 IEEE Ultrason. Symp.*, pp. 1125–1128.

[128] E. K. Sittig and G. A. Coquin, "Filters and dispersive delay lines using repetitively mismatched ultrasonics transmission lines", *IEEE Trans. Sonics Ultrason.*, Vol. SU-15, No. 2, April 1968, pp. 111–119.

[129] W. R. Smith, H. M. Gerard, J. H. Collins, T. M. Reeder, and H. J. Shaw, "Analysis of interdigital surface wave transducers by use of an equivalent circuit model", *IEEE Trans. Microwave Theory Tech.*, Vol. MTT-17, No. 11, November 1969, pp. 856–864.

[130] R. C. M. Li, "Analysis of surface wave reflection from a periodic array of electrodes", *Proc. 1972 IEEE Ultrason. Symp.*, pp. 263–266.

[131] R. C. M. Li and J. Melngailis, "The influence of stored energy at step discontinuities on the behavior of surface-wave gratings", *IEEE Trans. Son. Ultrason.*, Vol. SU–22, No. 3, May 1975, pp. 189–198.

[132] P. S. Cross, "Properties of reflective arrays for surface acoustic resonators", *IEEE Trans. Son. Ultrason.*, Vol. SU–23, No. 4, July 1976, pp. 255–262.

[133] J. R. Pierce, "Coupling of modes of propagation", *J. Appl. Phys.*, Vol. 25, No. 2, February 1954, pp. 179–183.

[134] Y. Koyamada and S. Yoshikawa, "Coupled mode analysis of a long IDT", *Review of the Electrical Communication Laboratories*, Vol. 27, No. 5–6, May–June 1979, pp. 432–444.

[135] D. Chen and H. A. Haus, "Analysis of metal-strip SAW gratings and transducers", *IEEE Trans. Son. Ultrason.*, Vol. SU–32, No. 3, May 1985, pp. 395–408.

[136] P. V. Wright, "A new generalized modeling of SAW transduders and gratings", *Proc. 43$^{rd}$ Freq. Contr. Symp.*, 31 May – 2 June 1989, pp. 596–605.

[137] V. P. Plessky, D. P. Chen and C. S. Hartmann, "'Patch' improvements to COM model for leaky waves", *Proc. 1994 IEEE Ultrason. Symp.*, pp. 297–300.

[138] A. R. Baghai-Wadji, F. Seifert, and K. Anemogiannis, "Rigorous analysis of STWs in nonperiodic arrays including mechanical and electrical interactions", *Proc. 1988 IEEE Ultrason. Symp.*, pp. 303–306.

[139] A. R. Baghai-Wadji and A. A. Maradudin, "Rigorous analysis of surface transverse waves in periodic arrays with arbitrary electroce profiles", *Proc. 1990 IEEE Ultrason. Symp.*, pp. 425–428.

[140] A. R. Baghai-Wadji, H. Reichinger, H. Zidek, and Ch. Mecklenbräuker, "Green's function applications in SAW devices", *Proc. 1991 IEEE Ultrason. Symp.*, pp. 11–20.

[141] R. C. Peach, "A general Green function analysis for SAW devices", *Proc. 1995 IEEE Ultrason. Symp.*, pp. 221–225.

[142] P. Bauerschmidt, R. Lerch, J. Machui, W. Ruile, and G. Visintini, "Reflection and transmission coefficients of SAW in a periodic grating computed by finite element analysis", *Proc. 1990 IEEE Ultrason. Symp.*, pp. 421–423.

[143] M. Buchner, W. Ruile, A. Dietz, and R. Dill, "FEM analysis of the reflection coefficient of SAWs in an infinite periodic array", *Proc. 1991 IEEE Ultrason. Symp.*, pp. 371–375.

[144] V. P. Plessky and T. Thorvaldsson, "Periodic Green's functions analysis of SAW and leaky SAW propagation in a periodic system of electrodes on a piezoelectric crystal", *IEEE Trans. Ultrason., Ferroelectr., Freq. Contr.*, Vol. 42, No. 2, March 1995, pp. 280–293.

[145] P. Ventura, J. Desbois, and L. Boyer, "A mixed FEM/analytical model of the electrode mechanical perturbation for SAW and PSAW propagation", *Proc. 1993 IEEE Ultrason. Symp.*, pp. 205–208; P. Ventura, J. M. Hodé, and M. Solal, "A new efficient combined FEM and periodic Green's function formalism for the analysis of periodic SAW structures", *Proc. 1995 IEEE Ultrason. Symp.*, pp. 263–268.

[146] G. Endoh, K. Hashimoto, and M. Yamaguchi, "Surface acoustic wave propagation characterisation by finite-element method and spectral domain analysis", *Japan. J. Appl. Phys.*, Vol. 34, Part 1, No. 5B, May 1995, pp. 2638–2641; K. Hashimoto and M. Yamaguchi, "General-purpose simulator for leaky surface acoustic wave devices based on coupling-of-modes theory", *Proc. 1996 IEEE Ultrason. Symp.*, pp. 117–122.

[147] J. Koskela, V. P. Plessky, and M. M. Salomaa, "Suppression of the leaky SAW attenuation with heavy mechanical loading", *IEEE Trans. Ultrason., Ferroelectr., Freq. Contr.*, Vol. 45, No. 2, March 1998, pp. 439–449.

[148] P. Ventura, J.-M. Hodé, M. Solal, J. Desbois, and J. Ribbe, "Numerical methods for SAW propagation characterization", *Proc. 1998 IEEE Ultrason. Symp.*, pp. 175–186.

[149] J. Ribbe, "On the coupling of integral equations and finite elements / Fourier modes for the simulation of piezoelectric surface acoustic wave components", PhD Thesis, CMAP / Ecole Polytechnique, 2002.

[150] J. V. Knuuttila, P. T. Tikka, C. S. Hartmann, V. P. Plessky, and M. M. Salomaa, "Anomalous asymmetric acoustic radiation in low-loss SAW filters", *Electr. Lett.*, Vol. 35, No. 13, 24 June 1999, pp. 1115–1116.

[151] J. Koskela, J. V. Knuuttila, P. T. Tikka, C. S. Hartmann, V. P. Plessky, and M. M. Salomaa, "Mechanism for acoustic leakage in surface-acoustic wave resonators on rotated Y-cut lithium tantalate substrate", *Appl. Phys. Lett.*, Vol. 75, No. 17, 25 October 1999, pp. 2683–2685.

[152] J. Koskela, J. V. Knuuttila, T. Makkonen, V. P. Plessky, and M. M. Salomaa, "Acoustic loss mechanisms in leaky SAW resonators on lithium tantalate", *IEEE Trans. Ultrason., Ferroelectr., Freq. Contr.*, Vol. 48, No. 6, November 2001, pp. 1517–1526.

[153] J. H. Collins, H. M. Gerard, K. M. Lakin, and H. J. Shaw, "100 MHz quartz delay line utilizing Rayleigh waves", *Proc. IEEE*, Vol. 56, No. 9, September 1968, pp. 1635–1636.

[154] J. H. Collins, H. M. Gerard, and H. J. Shaw, "High-performance lithium niobate acoustic surface wave transducers and delay lines", *Appl. Phys. Lett.*, Vol. 13, No. 9, 1 November 1968, pp. 312–313.

[155] T. W. Bristol, W. R. Jones, P. B. Snow, and W. R. Smith, "Applications of double electrodes in acoustic surface wave device design", *Proc. 1972 IEEE Ultrason. Symp.*, pp. 343–345.

[156] J. H. Rowen, "Tapped ultrasonic delay line and uses therefor", U. S. Patent 3,289,114, 29 November 1966.

[157] R. H. Tancrell, M. B. Schultz, H. H. Barrett, L. Davis, Jr., and M. G. Holland, "Dispersive delay lines using ultrasonic surface waves", *Proc. IEEE*, Vol. 57, No. 6, June 1969, pp. 1211–1213.

[158] R. H. Tancrell and M. G. Holland, "Acoustic surface wave filters", *Proc. IEEE*, Vol. 59, No. 3, March 1971, pp. 393–409.

[159] R. H. Tancrell and R. C. Williamson, "Wavefront distortion of acoustic surface waves from apodized interdigital transducers", *Appl. Phys. Lett.*, Vol. 19, No. 11, 1 Dec 1971, pp. 456–459.

[160] K. M. Lakin, T. Joseph, and D. Penunuri, "A surface acoustic wave planar resonator employing an interdigital electrode transducer", *Appl. Phys. Lett.*, Vol. 25, No. 7, 1 Oct 1974, pp. 363–365; K. M. Lakin, T. Joseph, and D. Penunuri, "Erratum: A surface acoustic wave planar resonator employing an interdigital electrode transducer", *Appl. Phys. Lett.*, Vol. 26, No. 6, 15 Mar 1975, p. 351.

[161] H. M. Gerard, "Acoustic scattering parameters of the electrically loaded interdigital surface wave transducer", *IEEE Trans. Microwave Theory Tech.*, Vol. MTT-17, No. 11, November 1969, pp. 1045–1046.

[162] E. Ash, "Surface wave grating reflectors and resonators", *Digest of IEEE Microwave Theory and Techniques Symp.* (1970), pp. 385–386.

[163] E. J. Staples, "UHF surface acoustic wave resonators", *Proc. 28th Freq. Contr. Symp.*, 29-31 May 1974, pp. 280–285; E. J. Staples, J. S. Schoenwald, R. C. Rosenfeld, and C. S. Hartmann, "UHF surface acoustic wave resonators", *Proc. 1974 IEEE Ultrason. Symp.*, pp. 245–252.

[164] T. R. Joseph, K. M. Lakin, and D. Penunuri, "Surface acoustic wave planar resonator using grating reflectors", *Appl. Phys. Lett.*, Vol. 26, No. 2, 15 January 1975, pp. 29–31.

[165] T. R. Joseph and K. M. Lakin, "Two-port cavity resonator low-insertion-loss delay line", *Appl. Phys. Lett.*, Vol. 26, No. 7, 1 Apr 1975, pp. 364–365; K. M. Lakin, T. Joseph, and D. Penunuri, "Planar surface acoustic wave resonators", *Proc. 1974 IEEE Ultrason. Symp.*, pp. 263–267.

[166] R. C. Williamson and H. I. Smith, "The use of surface-elastic-wave reflection gratings in large time-bandwidth pulse-compression filters", *IEEE Trans. Microwave Theory Tech.*, Vol. MTT-21, No. 4, Apr 1973, pp. 195–205.

[167] B. K. Sinha and H. F. Tiersten, "Variational analysis of the reflection of surface waves by arrays of reflecting strips", *J. Appl. Phys.*, Vol. 47, No. 7, July 1976, pp. 2824–2832.

[168] E. Cambiaggio, F. Cuozzo, and E. Rivier, "Finite difference analysis of piezoelectric surface wave behaviour on surface discontinuities: Application to acoustoelectric conversion in $LiNbO_3$ under a shielding conductor", *Proc. 1976 IEEE Ultrason. Symp.*, pp. 491–494; E. Cambiaggio and F. Cuozzo, "SAW reflection from conducting strips on $LiNbO_3$", *IEEE Trans. Son. Ultrason.*, Vol. SU–26, No. 5, September 1979, pp. 340–344.

[169] D. A. Simons, "Scattering of normally incident Rayleigh waves by thin strips", *J. Acoust. Soc. Am.*, Vol. 60, No. 5, November 1976, pp. 1100–1107.

[170] D. A. Simons, "Reflection of Rayleigh waves by strips, grooves, and periodic arrays of strips or grooves", *J. Acoust. Soc. Am.*, Vol. 63, No. 5, May 1978, pp. 1292–1301.

[171] S. Datta and B. J. Hunsinger, "First-order reflection coefficient of surface acoustic waves from thin-strip overlays", *J. Appl. Phys.*, Vol. 50, No. 9, September 1979, pp. 5661–5665.

[172] S. Datta and B. J. Hunsinger, "An analytical theory for the scattering of surface acoustic waves by a single electrode in a periodic array on a piezoelectric substrate", *J. Appl. Phys.*, Vol. 51, No. 9, September 1980, pp. 4817–4823.

[173] S. Datta and B. J. Hunsinger, "An analysis of storage effects on SAW propagation in periodic arrays", *IEEE Trans. Son. Ultrason.*, Vol. SU–27, No. 6, November 1980, pp. 333–341.

[174] K. Bløtekjær, K. A. Ingebrigtsen, and H. Skeie, "A method for analyzing waves in structures consisting of metal strips on dispersive media", *IEEE Trans. Electron. Dev.*, Vol. ED–20, No. 12, December 1973, pp. 1133–1138; K. Bløtekjær, K. A. Ingebrigtsen, and H. Skeie, "Acoustic surface waves in piezoelectric materials with periodic metal strips on the surface", *IEEE Trans. Electron. Dev.*, Vol. ED–20, No. 12, December 1973, pp. 1139–1146.

[175] T. L. Szabo, "Surface acoustic wave losses of thin-film gratings", *Appl. Phys. Lett.*, Vol. 22, No. 10, 15 May 1973, pp. 484–486.

[176] C. Dunnrowicz, "Reflection of surface waves from periodic discontinuities", *Proc. 1976 IEEE Ultrason. Symp.*, pp. 386–390.

[177] W. H. Haydl, P. Hiesinger, R. S. Smith, B. Dischler, and K. Heber, "Design of quartz and lithium niobate SAW resonators using aluminum metallisation", *Proc. $30^{th}$ Freq. Contr. Symp.*, 2–4 June 1976, pp. 346–357.

[178] G. L. Matthaei, F. Barman, and E. B. Savage, "S.A.W. reflecting arrays", *Electr. Lett.*, Vol. 12, No. 21, 14 October 1976, pp. 556–557.

[179] J. Temmyo, T. Inamura, and S. Yoshikawa, "Time domain observation of SAW reflection from a free aluminum metallized interface on $LiNbO_3$", *IEEE Trans. Son. Ultrason.*, Vol. SU–28, No. 1, January 1981, pp. 47–50.

[180] E. G. S. Paige, A. G. Stove, and R. C. Woods, "SAW reflection from aluminium strips on $LiNbO_3$", *Proc. 1981 IEEE Ultrason. Symp.*, pp. 144–147.

[181] P. V. Wright, "Modeling and experimental measurements of the reflection properties of SAW metallic gratings", *Proc. 1984 Ultrason. Symp.*, pp. 54–63.

[182] P. Ventura, "Full strip reflectivity study on quartz", *Proc. 1994 IEEE Ultrason. Symp.*, pp. 245–248.

[183] P. V. Wright and H. A. Haus, "Theoretical analysis of second-order effects in surface-wave gratings", *Proc. $34^{th}$ Freq. Contr. Symp.*, 28–30 May 1980, pp. 262–268.

[184] J. W. Cooley and J. W. Tukey, "An algorithm for the machine calculation of complex Fourier series", *Math. of Comput.*, Vol. 19, No. 90, April 1965, pp. 297–301.

[185] C. S. Hartmann and B. P. Abbott, "Experimentally determining the transduction magnitude and phase and the reflection magnitude and phase of SAW SPUDT structures," *Proc. 1990 IEEE Ultrasonics Symp.*, pp. 37–42.

[186] K. Yamanouchi and M. Takeuchi, "New types of SAW reflector and resonator with alternative (positive and negative) reflection coefficients", *Proc. 1986 IEEE Ultrason. Symp.*, pp. 224–228; K. Yamanouchi, M. Takeuchi, T. Meguro, and Y. Wagatsuma, "Positive/negative reflection-type SAW reflectors on ST-quartz using new fabrication technique", *Electr. Lett.*, Vol. 21, No. 21, 10 October 1985, pp. 966–968.

[187] M. Takeuchi and K. Yamanouchi, "New types of SAW reflectors and resonators consisting of reflecting elements with positive and negative reflection coefficients", *IEEE Trans. Ultrason., Ferroelectr., Freq. Contr.*, Vol. UFFC–33, No. 4, July 1986, pp. 369–374.

[188] D. P. Morgan, *Surface-wave devices for signal processing*, Elsevier, London, 1985, 432 p, see p. 377.

[189] K. Hashimoto, *Surface acoustic wave devices in telecommunications*, Springer, Berlin, 2000, 330 p, see pp. 26–27.

[190] V. P. Plessky and J. Koskela, "Coupling-of-modes analysis of SAW devices," pp. 1–82 in C. C. W. Ruppel and T. Fjeldly, *Advances in Surface Acoustic Wave Technology, Systems and Applications, Vol. 2*, World Scientific, 2001.

[191] H. Engan, "Interdigital electrode transducers for the excitation of elastic surface waves in piezoelectric media", Electronics Lab., Norwegian Institute of Technology, Trondheim, Norway, ELAB Rept. TE-91, September 1967.

[192] J. H. Collins, H. M. Gerard, T. M. Reeder, and H. J. Shaw, "Unidirectional surface wave transducer", *Proc. IEEE*, Vol. 57, No. 5, May 1969, pp. 833–835.

[193] J. C. Worley and H. Matthews, "Broadband unidirectional surface-wave transducer (Abstract in the 1970 IEEE Ultrasonics Symposium)", *IEEE Trans. Sonics Ultrason.*, Vol. SU-18, No. 1, January 1971, p. 52; *see also* [194].

[194] C. S. Hartmann, W. S. Jones, and H. Vollers, "Wideband unidirectional interdigital surface wave transducers", *IEEE Trans. Sonics Ultrason.*, Vol. SU-19, No. 3, July 1972, pp. 378–381.

[195] F. G. Marshall and E. G. S. Paige, "Novel acoustic-surface-wave directional coupler with diverse applications", *Electr. Lett.*, Vol. 7, No. 16, 12 August 1971, pp. 460–462; F. G. Marshall and E. G. S. Paige, "Observed properties of an acoustic-surface-wave multistrip coupler", *Electr. Lett.*, Vol. 7, No. 16, 12 August 1971, pp. 463–464.

[196] F. G. Marshall, C. O. Newton, and E. G. S. Paige, "Surface acoustic wave multistrip components and their applications", *IEEE Trans. Microwave Theory Tech.*, Vol. MTT-21, No. 4, April 1973, pp. 216–225.

[197] F. G. Marshall, E. G. S. Paige, and A. S. Young, "New unidirectional transducer and broadband reflector of acoustic surface waves", *Electr. Lett.*, Vol. 7, No. 21, 21 October 1971, pp. 638–640.

[198] R. S. Krimholtz, G. L. Matthaei, and B. E. Hoiem, "Acoustic-surface-wave interdigital hybrid-junction transducers", *IEEE Trans. Sonics Ultrason.*, Vol. SU-21, No. 1, January 1974, pp. 23–32.

[199] C. S. Hartmann, P. V. Wright, R. J. Kansy, and E. M. Garber, "An analysis of SAW interdigital transducers with internal reflections and the application to the design of single-phase unidirectional transducers", *Proc. 1982 IEEE Ultrason. Symp.*, pp. 40–45.

[200] K. Yamanouchi and H. Furuyashiki, "Low-loss SAW filter using internal reflection types of single-phase unidirectional transducer", *Electr. Lett.*, Vol. 20, No. 20, 27 September 1984, pp. 819–821.

[201] K. Yamanouchi and H. Furuyashiki, "Low-loss SAW filter using internal reflection types of new single-phase unidirectional transducer", *Proc. 1984 IEEE Ultrason. Symp.*, pp. 68–71.

[202] K. Yamanouchi, Z. H. Chen, and T. Meguro, "New fabrication technique for single-phase unidirectional SAW filter (EMUDT) in UHF range", *Electr. Lett.*, Vol. 21, No. 18, 29 August 1985, pp. 795–796.

[203] M. Lewis, "Low loss SAW devices employing single stage fabrication", *Proc. 1983 IEEE Ultrason. Symp.*, pp. 104–108; M. Lewis,"Group-type unidirectional SAW devices employing intra-transducer reflector banks", *Electr. Lett.*, Vol. 19, No. 25/26, 8 December 1983, pp. 1085–1087.

[204] P. V. Wright, "The natural single-phase unidirectional transducer: a new low-loss SAW transducer", *Proc. 1985 IEEE Ultrason. Symp.*, pp. 58–63.

[205] T. Kodama, H. Kawabata, Y. Yasuhara, and H. Sato, "Design of low-loss SAW filters employing distributed acoustic reflection transducers", *Proc. 1986 IEEE Ultrason. Symp.*, pp. 59–64.

[206] C. S. Hartmann and B. P. Abbott, "Overview of design challenges for single phase unidirectional SAW filters", *Proc. 1989 IEEE Ultrason. Symp.*, pp. 79–89.

[207] Y. Shui, J. M. Lin, H. Wu, N. Wang, and H. Chen, "Optimization of single-phase, unidirectional transducer using three fingers per period", *IEEE Trans. Ultrason., Ferroelectr., Freq. Contr.*, Vol. 49, No. 12, December 2002, pp. 1617–1621.

[208] K. Yamanouchi and H. Furuyashiki, "New low-loss SAW filter using internal floating electrode reflection types of single-phase unidirectional transducer", *Electr. Lett.*, Vol. 20, No. 24, 22 November 1984, pp. 989–990.

[209] K. Yamanouchi, T. Meguro, and K. Matsumoto, "Surface-acoustic-wave unidirectional transducers using anodic oxidation technology and low-loss filters", *Electr. Lett.*, Vol. 25, No. 15, 20 July 1989, pp. 958–960.

[210] K. Yamanouchi, "GHz-range unidirectional low-loss SAW filters and fine lithography technology", *Japan. J. Appl. Phys.*, Vol. 30, Supplement 30-1 (*Proceedings of 11th Symposium on Ultrasonic Electronics, Kyoto, 1990*), 1991, pp. 12–16.

[211] K. Yamanouchi, T. Meguro, and K. Matsumoto, "New electrode separation technology using anodic oxidation and application to SAW interdigital transducers", *IEEE Trans. Ultrason., Ferroelectr., Freq. Contr.*, Vol. 39, No. 3, May 1992, pp. 447–452.

[212] M. Takeuchi and K. Yamanouchi, "Coupled mode analysis of SAW floating electrode type unidirectional transducers", *IEEE Trans. Ultrason., Ferroelectr., Freq. Contr.*, Vol. 40, No. 6, November 1993, pp. 648–658.

[213] P. Ventura, M. Solal, P. Dufilie, J. M. Hodé, and F. Roux, "A new concept in SPUDT design: the RSPUDT (resonant SPUDT)", *Proc. 1994 IEEE Ultrason. Symp.*, pp. 1–6.

[214] H. Skeie and P. A. Nysen, "Surface acoustic wave passive transponder having acoustic wave reflectors", U. S. Patent 4,625,208, 25 November 1986.

[215] L. Reindl and W. Ruile, "Programmable reflectors for SAW-ID-tags", *Proc. 1993 IEEE Ultrason. Symp.*, pp. 125–130.

[216] K. Yamanouchi, G. Shimizu, and K. Morishita, "2.5 GHz-range SAW propagation and reflection characteristics and application to passive electronic tag and matched filter", *Proc. 1993 IEEE Ultrason. Symp.*, pp. 1267–1270.

[217] P. V. Wright, D. F. Thompson, and R. E. Chang, "Single-phase unidirectional transducers employing uniform-width dithered electrodes", *Proc. 1995 IEEE Ultrason. Symp.*, pp. 27–32.

[218] C.-Y. Jian and S. Beaudin, "A new type SPUDT SAW for use in high frequency around 2 GHz", *Proc. 2002 IEEE Ultrason. Symp.*, pp. 279–282.

[219] K. Yamanouchi, T. Meguro, Y. Wagatsuma, and H. Satoh, "High temperature stable GHz-range low-loss wide band transducers and filter using $SiO_2$/$LiNbO_3$,$LiTaO_3$", *Proc. 1991 IEEE Ultrason. Symp.*, pp. 137–140.

[220] G. Martin, H. Schmidt, and B. Wall, "New SPUDT cell structures", *IEEE Trans. Ultrason., Ferroelectr., Freq. Contr.*, Vol. 51, No. 7, July 2004, pp. 859–864.

[221] C. S. Hartmann, "A global SAW ID tag with large data capacity", *Proc. 2002 IEEE Ultrason. Symp.*, pp. 65–69.

[222] C. S. Hartmann, P. Brown, and J. Bellamy, "Design of global SAW RFID tag devices," *Proc. Second International Symposium on Acoustic Wave Devices for Future Mobile Communications Systems*, Chiba University, Chiba, Japan, March 3-5, 2004, pp. 15-19.

# Abstracts of Publications I–VII

**I** In this work, we study theoretically the operation of long surface acoustic wave reflectors, comprising a large number of electrodes, at the fundamental and second harmonic frequencies on the 128° $LiNbO_3$ substrate for various electrode thicknesses and metallization ratios. Numerical simulations utilizing tailored test structures and time gating indicate that the reflectivity of the second-harmonic reflectors can be very high for certain geometries. Furthermore, our simulations suggest that inside the stopband the total losses for the second harmonic are of the same order as those for operation at the fundamental harmonic.

**II** In this work, we study numerically the operation of surface acoustic wave (SAW) reflectors comprising a small number of electrodes on the 128° YX-cut lithium niobate ($LiNbO_3$) substrate. The electrodes have a finite thickness, and they are either open circuited or grounded. The center-to-center distance between adjacent electrodes $d$ corresponds roughly either to half of the characteristic wavelength $d \propto \lambda_0/2$ or to $d \propto \lambda_0$, for the reflectors operating at the fundamental and second harmonic modes, respectively. We use software based on the finite-element and boundary-element methods (FEM/BEM) for numerical experiments with a tailored test structure having 3 interdigital transducers (IDTs), simulating experimental conditions with an incident wave and reflected and transmitted SAWs. Using the fast Fourier transform (FFT) and time-gating techniques, calculation of the Y-parameters in a wide frequency range with rather a small step allows us to determine the reflection coefficients, and to estimate the energy loss due to bulk-wave scattering. The detailed dependences of the attenuation and reflectivity on the metallization ratio and the electrode thickness are given for the classic 128°-cut of $LiNbO_3$.

**III** We consider the interaction of surface acoustic waves (SAWs) with short electrode gratings encompassing only few electrodes on 128° lithium niobate ($LiNbO_3$). The qualifications of the reflectors are evaluated by comparing the part of incident SAW energy scattered by the structure into the bulk to the energy reflected back as a SAW.

**IV** We study numerically the phase of surface acoustic waves reflected by or transmitted through short reflectors comprising only 1–3 aluminium electrodes on 128° YX-cut $LiNbO_3$. The electrodes have a finite thickness and they are either open-circuited or grounded. The center-to-center distance between adjacent electrodes $d$ corresponds roughly either to half of the characteristic wavelength $d \propto \lambda_0/2$ or to $d \propto \lambda_0$, for the reflectors operating at the fundamental and second harmonic modes, respectively. We use software based on the finite-element and boundary-element methods (FEM/BEM) for numerical experiments with a tailored 3-IDT test structure, simulating experimental conditions with an incident wave and reflected and transmitted SAWs. Employing artificial enhancement of time resolution in conjunction with the fast Fourier transform (FFT) and time-gating, calculation of the Y-parameters in a relatively wide frequency range allows us to determine the phase of the reflection and transmission coefficients.

**V** In this paper, the extraction of the coupling-of-modes (COM) model attenuation parameter $\gamma$ in a finite grating is considered. We use test structures comprising identical transmitting and receiving transducers and a grating centered in the acoustic channel along the propagation direction of the surface acoustic wave (SAW). The extraction procedure is based on studying the magnitude of the ratio of the reflection and transmission coefficients of the grating, R/T, obtained through time gating from the S parameter measurements of the test devices. In particular, it is found that the level of the notches of R/T directly depends on the attenuation of SAW in the grating. A simple closed-form expression for the attenuation normalized to the grating length, $\gamma\lambda_0$, depending on the characteristics of |R/T|, is given. The extracted attenuation is presented as a function of the thickness ($h/\lambda_0$) and the metallisation ratio ($a/p$).

**VI** A single-phase unidirectional transducer (SPUDT) structure using $\lambda/4$ and wider electrodes is introduced. The considerable difference between the reflectivity of short-circuited $\lambda/4$ electrodes and that of floating $\lambda/2$-wide electrodes on 128° lithium niobate ($LiNbO_3$) is exploited. The surface acoustic wave (SAW) device operating at 2.45 GHz has critical dimensions of about 0.4 $\mu$m, accessible for standard optical lithography.

**VII** Filters based on employing single-phase unidirectional transducers (SPUDTs) consisting of $\lambda/4$ and wider electrodes are presented. The design variants exploit the significant difference between the reflectivity of short-circuited $\lambda/4$ electrodes and that of floating wide electrodes on 128° $LiNbO_3$. The SAW devices operating at 2.45 GHz have critical dimensions of about 0.4 $\mu$m, accessible to standard optical lithography. When matched, the fabricated SPUDT filters exhibit minimum insertion losses of 5.5–7.9 dB together with 3 dB passbands of 89–102 MHz. The majority of the insertion loss can be attributed to the attenuation on free surface and inside the grating, and to the resistivity of the electrodes.